

ESULAB

2024

3rd European Symposium on Ultrafast Laser driven Biophotonics

September 15 – 18
Volkshaus Jena // Germany

Poster Abstracts

Organized by



Funded by



Sponsored by



Fiber-laser driven spectroscopy & imaging from the MIR to the XUV

Sven Breitkopf, Vinzenz Hilbert, Maxim Tschernajew, Christian Grebing, Anke Heilmann, Evgeny Shestaev, Christian Gaida, Tino Eidam and Jens Limpert

Active Fiber Systems GmbH, Ernst-Ruska-Ring 17, 07745 Jena, Germany

publications@afs-jena.de

Abstract for EsuLAB 2024 in Jena, Germany, ©Active Fiber Systems GmbH

Introduction

Ytterbium- and Thulium-based fiber laser systems are an excellent choice as a seeding source for multiple frequency-conversion techniques. Due to their high-power capabilities they allow for significant power- and flux-levels even for techniques with relatively low conversion-efficiencies such as high-harmonic generation. We will present different techniques based upon fiber-laser systems, allowing for imaging and spectroscopy applications at unprecedented measurement speeds.

High-flux XUV sources for ARPES and CDI

Sources of short-wavelength radiation, such as synchrotrons or free-electron lasers, have already enabled numerous applications and will facilitate more seminal studies. In recent years, sources of coherent extreme ultraviolet to soft x-ray radiation via high-harmonic generation (HHG) of ultrashort-pulse lasers have gained significant attention due to their enormous potential to address a plethora of applications in a cost-effective and tabletop format [1]. Therefore, they constitute a complementary source to large-scale facilities. The photon-flux values obtained by fiber-laser-driven HHG sources can be considered the highest of all laser systems for photon energies between 20-150 eV. Fiber lasers with high repetition-rates are ideal high-harmonic drivers. These turnkey HHG beamlines can address several applications in the EUV to X-ray spectral region and are widely used for angle-resolved photoemission spectroscopy (ARPES) [2], coherent-diffractive imaging (CDI) [3] and a vast number of other techniques.

Mid-IR sources for the molecular fingerprint-region

Frequency combs in the molecular fingerprint region have enabled applications in metrology, spectroscopy and medicine. All these applications benefit from higher average powers that allow for faster acquisition rates and an improved signal-to-noise ratio. Ultrafast mid-IR pulses with a tunable central wavelength between 5 μ m to 18 μ m can be achieved through intra-pulse difference-frequency generation, which guarantees passive carrier-envelope-offset stability. The complete frequency-comb nature of the source can be achieved by controlling and stabilizing the fundamental pulse-repetition frequency of the driving laser [4]. Starting from a compact 50fs-thulium-doped ultrafast fiber-laser system this technique can provide a high-power frequency comb in the mid-IR.

Tunable and compact CARS and SRS sources

Coherent anti-Stokes Raman and Stokes Raman spectroscopy are popular techniques based on a vibrational contrast mechanism to analyze biological samples. Compact, alignment-free and all-fiber picosecond laser source for CARS microscopy delivering synchronized pump and Stokes pulses from a single fiber end can offer a versatile approach to help bringing these techniques from university laboratories into clinical studies. This air-cooled and turn-key CARS laser source has a great benefit for the user as the fiber delivery eliminates alignment of the spatial and temporal pulse overlap. High quality and high-speed microscopic multimodal nonlinear imaging is possible by e.g. simultaneously probing the CARS CH-vibrational-levels of lipids around 2850 cm^{-1} , the second harmonic generation (SHG) and the two-photon excited fluorescence (TPEF) signals [5].

Ultrafast THz sources at the highest average power levels

Radiation in the Terahertz spectral region is of growing interest. However, THz sources with high power levels are hardly available. Thus, THz particle acceleration, the studies of nonlinear effects and material properties, pump-probe experiments, spectroscopy of aqueous samples and many other applications would significantly profit from novel high-power sources in the THz gap. Using fiber-lasers and relatively simple frequency conversion mechanisms can allow for significant upscaling of the available flux in the THz region. Up to 50 mW have been recently demonstrated using such techniques [6].

Conclusion

High-power ytterbium- and thulium-based fiber laser systems can be employed to generate radiation that covers a remarkable wavelength range, enabling a vast number of imaging and spectroscopy applications starting from the XUV-regime all the way to the THz-region.

References

- [1] R. Klas, S. Demmler, M. Tschernajew, S. Hädrich, Y. Shamir, A. Tünnermann, J. Rothhardt, and J. Limpert, "Table-top milliwatt-class extreme ultraviolet high harmonic light source," *Optica* 3, 1167 (2016).
- [2] Andrea Damascelli, "Probing the Electronic Structure of Complex Systems by ARPES", *Physica Scripta T109*, 61-74 (2004)
- [3] J. Rothhardt, G. Tadesse, W. Eschen, and J. Limpert, "Table-top nanoscale coherent imaging with XUV light", *Journal of Optics* 20, 113001 (2018).
- [4] C. Gaida, M. Gebhardt, T. Heuermann, F. Stutzki, C. Jauregui, J. Antonio-lopez, A. Schülzgen, R. Amezcua, A. Tünnermann, I. Pupeza and J. Limpert "Watt-scale super-octave mid-infrared intrapulse difference frequency generation," *Light Sci. Appl.* 1–11 (2018).
- [5] T. Gottschall, T. Meyer, M. Baumgartl, C. Jauregui, M. Schmitt, J. Popp, J. Limpert, and A. Tünnermann, "Review: fiber-based light sources for biomedical applications of coherent anti-Stokes Raman scattering microscopy," *Laser Photon. Rev.* 9, 435–451 (2015).
- [6] Joachim Buldt, Michael Müller, Henning Stark, Cesar Jauregui and Jens Limpert, "Average-Power Scaling of Broadband THz radiation to 50 mW", Conference distribution at IRMMW 2019 in Paris (2019)

Surface enhanced coherent anti-Stokes Raman scattering and nonlinear signal generation on plasmonic chirped gratings

Jer-Shing Huang

Research Department of Nanooptics, Leibniz Institute of Photonic Technology, 07745 Jena, GERMANY

Email: jer-shing.huang@lebniz-ipht.de

The capability to control light enables the manipulation and enhancement of light-matter interaction. Rationally designed nanostructures can function as optical antennas to control optical fields, and thereby enhance light-matter interaction, especially nonlinear signal and coherent Raman scattering where intensified optical field is a necessary. In this presentation, I will present our recent progress in surface-enhanced coherent anti-Stokes Raman scattering (SECARS) [1], second harmonic generation (SHG) [2], two-photon photoluminescence (TPPL), and four-wave mixing (FWM) [3] using smartly designed plasmonic chirped gold gratings (Fig.1) [4], which is also of great potential for spectrometer-free optical sensing [5-6]. The enhancement mechanisms for SECARS, SHG, TPPL and FWM will be presented with verification using theoretical analysis and numerical simulations.

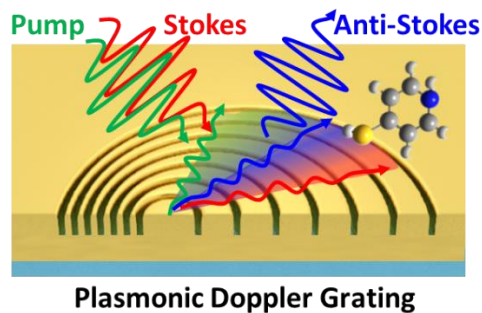


Figure 1. An azimuthally chirped plasmonic gold grating enables spatial resolved investigation of the enhancement mechanism of in surface-enhanced coherent anti-Stokes Raman scattering, second harmonic generation, two-photon photoluminescence, and four-wave mixing.

References

1. "Spatially Resolving the Enhancement Effect in Surface-Enhanced Coherent Anti-Stokes Raman Scattering by Plasmonic Doppler Gratings" Ouyang, L.; Meyer, T.; See, K.-M.; Chen, W.-L.; Lin, F.-C.; Akimov, D.; Ehtesabi, S.; Richter, M.; Schmitt, M.; Chang, Y.-M.; Gräfe, S.; Popp, J.; Huang, J.-S.* *ACS Nano*, **2021**, *15*, 809-818.
2. "Nonlinear optical signal generation mediated by a plasmonic azimuthally chirped grating" Barman, P.; Chakraborty, A.; Akimov, D.; Singh, A. K.; Meyer-Zedler, T.; Wu, X.; Ronning, C.; Schmitt, M.; Popp, J.*; Huang, J.-S.* *Nano Lett.*, **2022**, *22*, 9914-9919.
3. "Broadband Four-Wave Mixing Enhanced by Plasmonic Surface Lattice Resonance and Localized Surface Plasmon Resonance in an Azimuthally Chirped Grating" Chakraborty, A.; Barman, P.; Singh, A. K.; Wu, X.; Akimov, D. A.; Meyer-Zedler, T.; Nolte, S.; Ronning, C.; Schmitt, M.; Popp, J.* and Huang, J.-S.* *Laser & Photonics Reviews* **2023**, *17*, 2200958.
4. "Design and Characterization of Plasmonic Doppler Grating for Azimuthal Angle-resolved Surface Plasmon Resonances" See, K.-M.; Lin, F.-C.; Huang, J.-S.* *Nanoscale* **2017**, *9*, 10811-10819.
5. "Designable spectrometer-free index sensing using plasmonic Doppler gratings" Lin, Fan-Cheng; See, Kel-Meng; Huang, You-Xin; Chen, Yi-Ju; Ouyang, Lei; Popp, Jürgen; Huang, Jer-Shing* *Anal. Chem.*, **2019**, *91*, 9382-9387.
6. "Spectrometer-free optical hydrogen sensing based on Fano-like spatial distribution of transmission in a metal-insulator-metal plasmonic Doppler grating" Chen, Y.-J.; Lin, F.-C.; Singh, A. K.; Ouyang, L.; Huang, J.-S.* *Adv. Opt. Mater.* **2021**, *9*, 2100869.

Biomarker Detection: Implementation of Raman Fingerprint Profiles in Multi-OMICs Data Analysis

Katerina Prohaska*, Daniel Zimmermann, David Lilek, Agnes Grünfelder, Christoph Großinger, Alfred Minarik, Justyna Rechthaler, and Birgit Herbinger
Biotech Campus Tulln of FH Wiener Neustadt, Tulln, Austria

* Corresponding Author: Katerina Prohaska, E-Mail: Katerina.prohaska@fhwn.ac.at

Abstract.

With as many as 14 million new cases and over 8.8 million deaths each year around the globe, cancer is considered one of the most devastating diseases in modern times. As such, there is a prominent driving force to develop efficient workflows and tools for faster and more accurate diagnosis.

Multi-omics is particularly interesting in cancer research because it allows for a comprehensive understanding of the disease by integrating data from various biochemical layers. By combining proteomics, metabolomics, transcriptomics and spectralomics by Raman spectroscopy, we aim to identify novel biomarkers for early detection and targeted therapy.

Here, we investigated the response of Hodgkin Lymphoma cells to two-substance treatment with Etoposide and Resveratrol. The chemotherapeutic Etoposide, primarily inducing substantial DNA damage, serves to trigger apoptosis in cancer cells. Resveratrol, the natural constituent of many foods such as wine grapes, displays potential inhibitory effects on carcinogenesis through multifaceted targeting mechanisms, thereby augmenting apoptotic pathways [1].

It has been observed that certain epigenetic changes, such as DNA methylation, as well as metabolic alterations can contribute to the development of cancer and are thus recognized as potential additional biomarkers for diagnosis. Metabolites such as succinate, fumarate and 2-hydroxyglutarate act as oncogenic signals (oncometabolites) and are therefore suggested to be used as powerful biomarkers for diagnosing and monitoring cancer [2]. Our goal is to investigate epigenetic and metabolic changes of Hodgkin Lymphoma cells using a multi-omics approach.

Cancer cells exhibit accelerated proliferation rates, leading to heightened frequency of DNA replication. While tumor suppressor proteins like p53 are pivotal in normal cellular function, their dysregulation in cancer cells, including the HL cell line L-428 which harbors a mutation in the p53 gene, underscores the intricate interplay between genetic alterations and oncogenic processes.[3] Additionally to studying the cell line L-428 we also investigated the p53 wildtype HL line L-540 and addressed the therapeutic success of Etoposide combined with Resveratrol in both cell lines (Figure 1).

To assess the effectiveness of the two-substance therapeutic treatment four scientific disciplines delivered method specific data sets. To enable a valid biological interpretation advanced computational tool like the “regularized generalized canonical correlation analysis” (RGCCA) for the multi-omics analysis must be selected and its application evaluated.[4, 5]

We aim to correlate the overexpressed genes detected in the qPCR analysis and the molecular chemical SERS fingerprint reflecting the overall cell status, as well as to map the protein identifications to gene ontology terms of biological processes, molecular functions and cellular compartments derived from bottom-up proteomics approach by applying Nano-LC-MS/MS technique. In addition, the profiles of metabolites, the small molecules involved in metabolic pathways, detected by GC-MS analysis will be linked to the knowledge gained. [6–8]

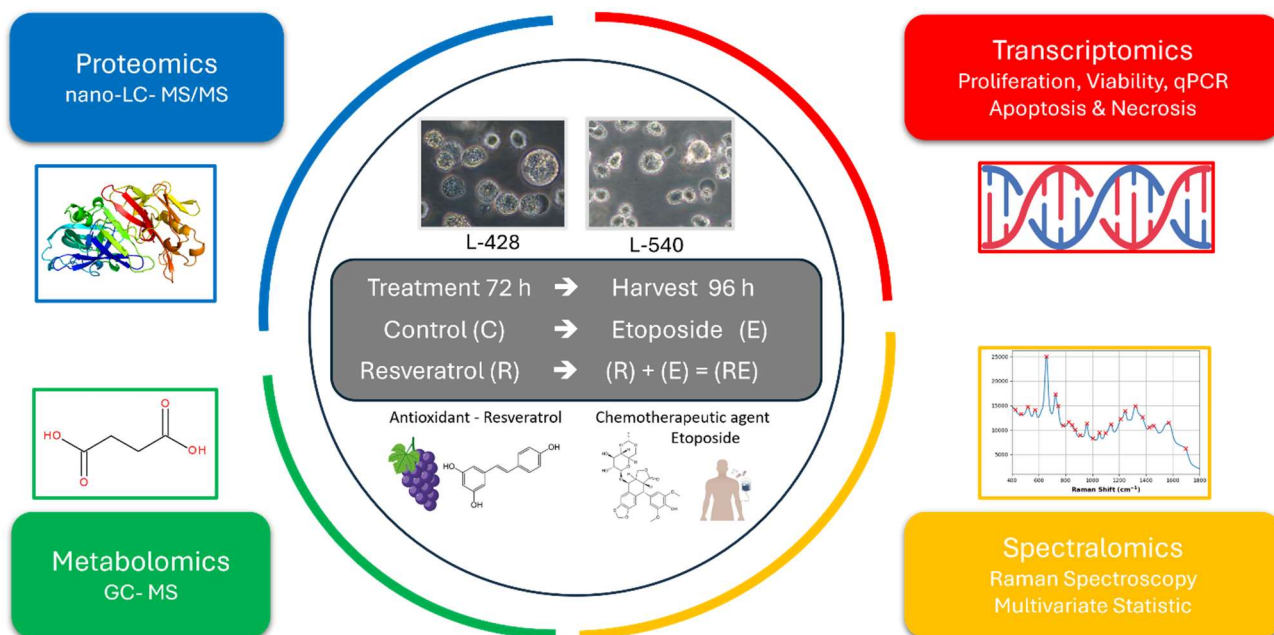


Figure 1: Experimental Setup for Biomarker detection: Data sets and Analytics; time scale and sequence of treatments is depicted by white arrows.

Literature:

1. Prohaska K, Zimmermann D, Lilek D, Grünfelder A, Herbinger B (2022) Raman Analytics to Monitor Influence of Resveratrol on Lymphoma Cells. In: Villach FFH 2022
2. Collins RRJJ, Patel KG, Putnam WC, Kapur P, Rakheja D (2017) Oncometabolites: A New Paradigm for Oncology, Metabolism, and the Clinical Laboratory. Clin Chem 63:1812–1820. <https://doi.org/10.1373/clinchem.2016.267666>
3. Zimmermann D, Lilek D, Herbinger B, Prohaska K (2023) Comparison of different machine learning algorithms for fast and interpretable evaluation of Raman spectroscopic data. In: Anakon 2023. Vienna, Austria, pp 12–19
4. Revilla L, Mayorgas A, Corraliza AM, Masamunt MC, Metwaly A, Haller D, Tristán E, Carrasco A, Esteve M, Panés J, Ricart E, Lozano JJ, Salas A (2021) Multi-omic modelling of inflammatory bowel disease with regularized canonical correlation analysis. PLOS ONE 16:e0246367. <https://doi.org/10.1371/journal.pone.0246367>
5. Subramanian I, Verma S, Kumar S, Jere A, Anamika K (2020) Multi-omics Data Integration, Interpretation, and Its Application. Bioinforma Biol Insights 14:7–9. <https://doi.org/10/ggn3c8>
6. Zimmermann D, Lilek D, Minarik, A, Herbinger B, Prohaska K (2023) Metabolic changes in chemotherapeutically treated Hodgkin Lymphoma cells: complementary analytics by SERS and GC-MS. In: Data4OMICs Symposium 2023. Tulln, Austria
7. Zimmermann D, Lilek D, Posch N, Hermann D-R, Pytel N, Herbinger B, Prohaska K (2023) Classification of single cells by Raman spectroscopy and machine learning: comparison of common algorithms. In: Scientific Computing 2023. Graz, Austria
8. Rudolf-Scholik J, Lilek D, Maier M, Reischenböck T, Maisl C, Allram J, Herbinger B, Rechthaler J (2024) Increasing protein identifications in bottom-up proteomics of *T. castaneum* – Exploiting synergies of protein biochemistry and bioinformatics. J Chromatogr B 1240:124128. <https://doi.org/10.1016/j.jchromb.2024.124128>

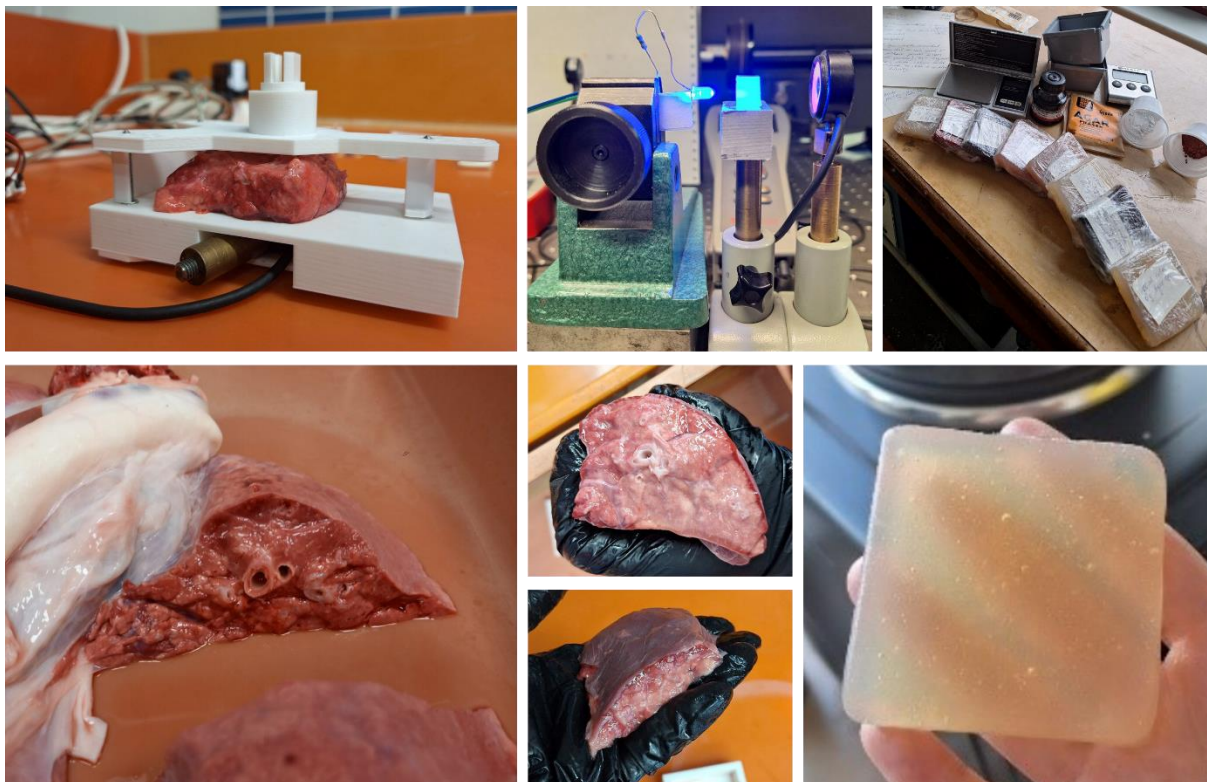
EFFECT OF LUNG DEGRADATION ON ITS OPTICAL PROPERTIES AND AGAR-BASED OPTICAL PHANTOM FABRICATION

Finaeva Uliana^{1,*}, Sarka Nemcova¹, Petr Denk¹, Jiri Cap¹

1. Czech Technical University in Prague, Faculty of Mechanical Engineering, Department of Instrumentation and Control Engineering, Division of Precision Mechanics and Optics, Technicka 4, Prague 6, 160 00, Czech Republic

* uliana.finaeva@fs.cvut.cz

This study focuses on two primary objectives: analysing the effect of degradation on the optical properties of pig lung tissue and developing agar-based optical phantoms aimed at mimicking lung tissue. We compared relatively freshly removed pork lung tissue to tissue refrigerated for three days to understand storage and degradation impacts to the optical properties of the biomaterial samples. To create phantoms, we used easily accessible cooking agar matrix base and affordable scattering agents such as polishing sands and ink, this being inspired by Ntombela's work from year 2002. Two batches of phantoms were prepared to examine recipe differences and concentration effects. Wavelength of the light source (LEDs) for measurement of transmission and scattering varied from 475 to 950 nm. Our results, as well as others reported in literature, show variability, highlighting the complexity of tissue behaviour and the need for standardized and detailed prescriptions for measurement procedures as well as sampling of the tissue. This study provides insights for future medical optics research and development.



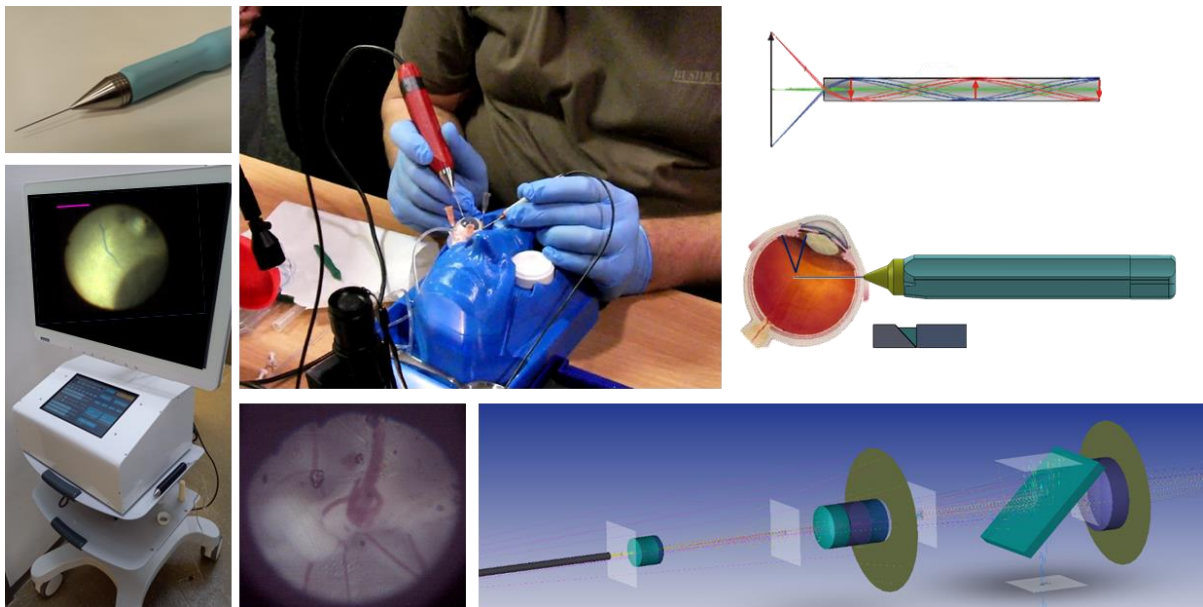
Ophthalmic endoscope

Nemcova Sarka^{1, *}, Finaeva Uliana¹, et al.

1. Czech Technical University, Prague, Czech Republic,

sarka.nemcova@fs.cvut.cz

Author and team members present a full process of development of the ophthalmic endoscope from scratch. The developed tool is supposed to be used for diagnostic and treatment in difficult situations, where the eye is not transparent (due to injury or disease), and the standard operation microscope cannot be used. Developed system's prototype with 23-gauge probe momentarily allows visualization of the posterior and anterior segment of an eye including visualization of the ciliary muscles, otherwise not accessible by the microscope. Camera image consists of 360 000 pixels, field of view is 36-degrees and resolution of the system is up to 20 micrometres at 3 mm working distance. The principle of the device allows even better resolution, as optical fibers limitations are not applicable to the case. At this stage project status is ongoing and working prototype with the image optical path is fully tested on a pig's eye. Laser optical path is implemented and will be further tested this year. The whole design meets the Medical Device Regulation requirements, however, is not medically certified yet. The demonstrated prototype is a result of several years' work of interdisciplinary scientists and engineering students in Czech Republic led by the author's passion and experience. Management and directing of such project are one of the key processes of developing the manufacturable, robust and handy medical diagnostic tool. Challenges met along the way and ways to overcome them are to be presented at the poster section at ESULAB 2024 Biophotonics For Future Conference.



Widely tunable laser source with spectrally-compressed linewidth for long-wavelength optical coherence tomography at 1700 nm

Olga Szewczyk, Grzegorz Soboń

Laser & Fiber Electronics Group, Wrocław University of Science and Technology, 50-370 Wrocław, Poland

Rapidly tunable laser sources with narrowed linewidth can be used in various areas such as metrology, spectroscopy, and optical coherence tomography (OCT). They can be useful especially for the OCT as swept sources offer very narrow instantaneous bandwidth and wide sweeping range. It has already been shown that the 1700 nm spectral window can serve as an alternative to the commonly utilized 1300 nm wavelength bandwidth, offering lower scattering in tissue and, therefore, increased penetration depth [1]. By combining nonlinear effects in optical fibers to obtain a tunable laser source, and a specially designed spectral compression technique to narrow the linewidth of the generated pulses, it is possible to realize an all-fiber laser source with parameters adjusted for long-wavelength OCT.

The laser source incorporates an Erbium-doped fiber laser that serves as a seed generating 40-fs pulses at a 50 MHz repetition rate with 250 mW maximum average optical power. The pulses from the seed laser are then provided to a polarization-maintaining single-mode fiber (PM-SMF) which enables spectral conversion of the pulses up to 1900 nm due to the soliton self-frequency shift (SSFS) effect. The optical spectra of the generated pulses are presented in Fig. 1 (a). The tunable pulses, so-called optical solitons, possess too large spectral widths (between 14.9-16.2 nm) to be used for OCT, and, hence, require narrowing. The spectral compression is achieved in a fiber that features varying dispersion profiles, a comb-profile fiber (CPF). The CPF is realized by combining different segments of SMF and dispersion-shifted fiber (DSF) in a pattern that was previously designed numerically. This allows for the frequency-shifted pulses to be narrowed to the levels of 0.43–1.11 nm. The optical spectra are depicted in Fig. 1 (b). Lastly, the spectrally-shifted solitons are amplified in the Thulium-doped fiber amplifier to ensure satisfactory power levels for further OCT analysis. The laser system contains an electro-optic modulator that allows for rapid sweep up to 10 GHz. To summarize, the narrow-linewidth laser system meets the requirements for OCT and can be used for biomedical imaging.

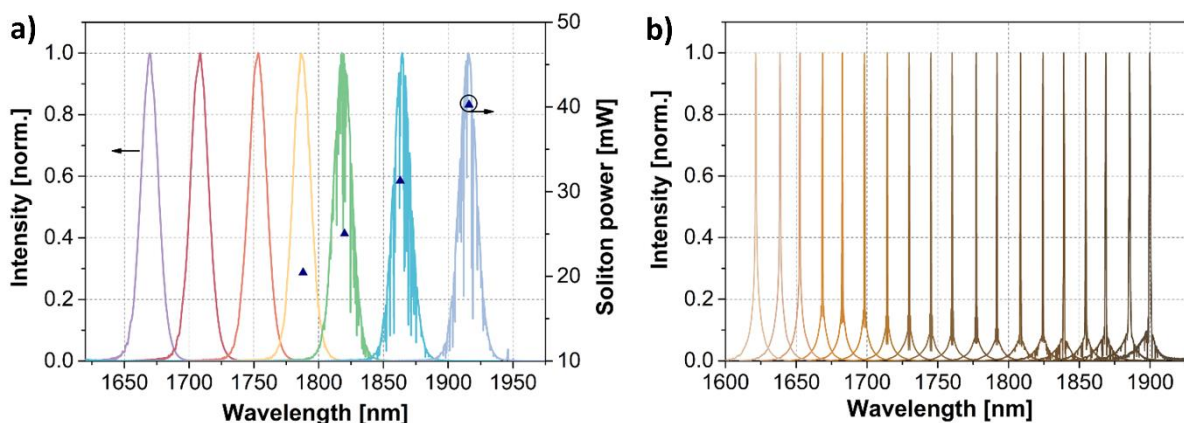


Fig. 1. Optical spectra of the tunable solitons before (a) and after spectral compression (b).

References:

- [1] D. R. Miller, J. W. Jarrett, A. M. Hassan, and A. K. Dunn, "Deep tissue imaging with multiphoton fluorescence microscopy," *Curr. Opin. Biomed. Eng.* 4, 32–39 (2017).

Enhancing multiphoton microscopy with picosecond pulses

Katarzyna Kunio[#], Jakub Boguslawski, Grzegorz Sobon

Laser & Fiber Electronics Group, Faculty of Electronics, Photonics and Microsystems,
Wrocław University of Science and Technology, Wybrzeże Wyspiańskiego 27, 50-370 Wrocław, Poland
[#]corresponding author email: katarzyna.kunio@pwr.edu.pl

Multiphoton microscopy [1] is a sophisticated imaging method that employs multiple lower-energy photons to excite fluorophores, allowing for deeper tissue penetration and minimized photodamage compared to traditional fluorescence microscopy. This technique enables precise visualization of cellular structures and dynamic processes in intact biological samples through nonlinear optical processes. Ti:sapphire lasers [2] are commonly used for this purpose due to their short pulse durations and high peak powers; however, they are also bulky, complex, and costly. Additionally, their short pulses can broaden because of dispersive optical elements in the microscope, requiring careful dispersion management to maintain excitation efficiency. We propose an efficient multiphoton microscopy setup using a 10 nJ Yb: fiber laser that generates picosecond pulse trains. This setup can achieve performance comparable to femtosecond pulse trains by reducing the pulse repetition rate (f_{rep}) while being less affected by chromatic dispersion. This suggests that a compressor is not always necessary and can be replaced with a smaller, more user-friendly all-fiber setup.

Figure 1(a) shows the schematic of our experimental multiphoton microscopy setup. We have constructed a self-starting, all-PM, Yb: fiber oscillator consisting of two cavity sections: the main loop and the nonlinear amplification loop mirror (NALM). Each loop is pumped with a 976 nm laser diode. The NALM loop incorporated a reflection-type wavelength-division multiplexer (WDM) and an asymmetrically placed active Yb-doped fiber (YDF). The main loop consisted of a YDF, an isolator (ISO), a WDM, a 10-nm bandpass filter (BP), and a fiber coupler that directed 70% of the optical power out of the system. The laser produces high-energy pulses (~ 10 nJ) with a central wavelength of 1026.5 nm [Fig. 1(b)]. The duration of one pulse was equal to 10.1 ps [Fig. 1(c)]. The f_{rep} was equivalent to 15.23 MHz and the oscillator could be characterized by good stability, as shown in Fig. 1(d). Figure 1(e) shows the RIN equal to 0.53% root-mean-square measured in the range of 10 Hz to 3 MHz. This measurement was conducted in laboratory conditions, with no thermal stabilization.

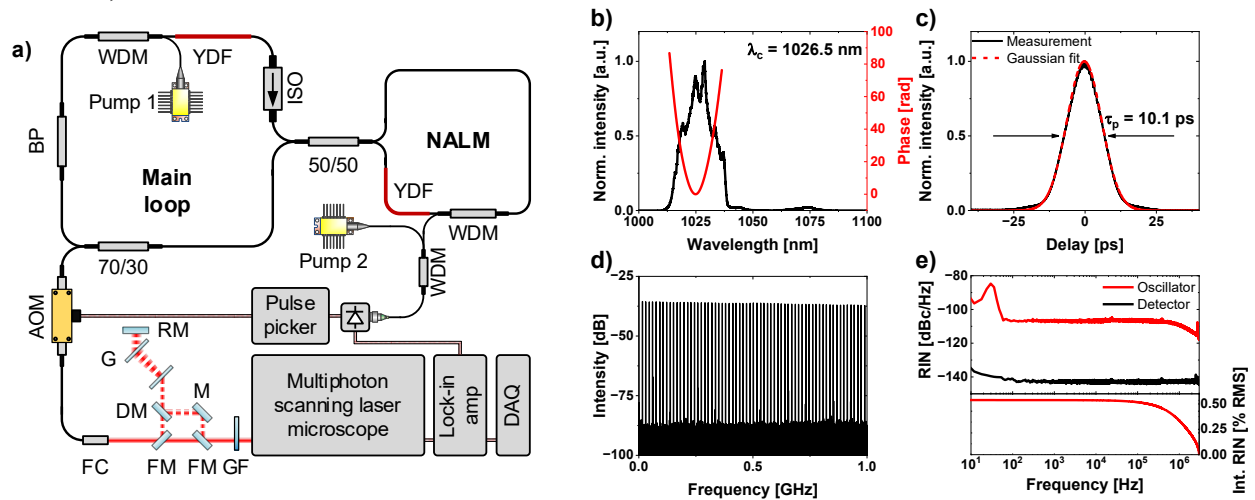


Fig. 1. a) Schematic of the experimental setup. BP – bandpass filter, YDF – Yb-doped fiber, WDM – wavelength-division multiplier, ISO – isolator, AOM – acousto-optic modulator, FC – fiber collimator, FM – flip mirror, DM – D-shaped mirror, G – diffraction grating, RM – retro mirror, M – mirror, GF – gradient index filter, DAQ – data acquisition card. Characterization of the Yb: fiber oscillator: b) the optical spectrum with the spectral phase, c) autocorrelation of the pulse with the Gaussian fit, d) the RF spectrum, e) RIN and integrated RIN.

The oscillator is then connected to the pulse picking unit used to reduce the f_{rep} of the pulse train. The pulse picker consists of an acousto-optic modulator (AOM) and an electronic driver and it transmits the pulses synchronously with the oscillator thanks to the photodiode connected to the previously unused port in the WDM. Then, the beam is collimated and can either be directed through a typical Treacy compressor (estimated group delay dispersion of -1.17 ps² and transmission of 79%) or it can be led into the multiphoton scanning laser microscope [3] connected to the lock-in amplifier to ensure better image quality. In the end, the demodulated signal is sampled using the data acquisition card (DAQ).

Figures 2(a)-(b) show the pico- and femtosecond pulse trains before and after propagation through the microscopy system, respectively. The duration of the picosecond pulse at the sample plane was equal to 10.31 ps and it was not affected by the chromatic dispersion of the microscopy setup. However, the duration of the femtosecond pulse after going through the microscope was elongated to 227 fs and its peak power decreased by ~35% with respect to the peak power of the pulse before transmission through the microscope.

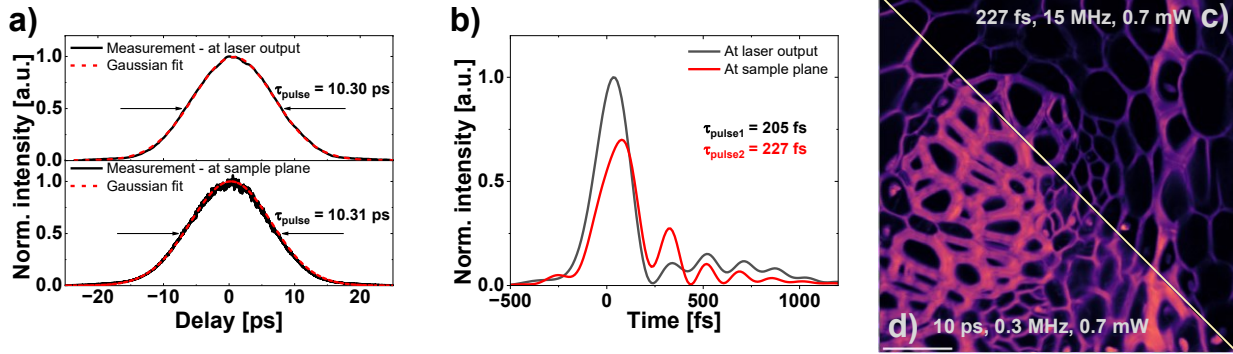


Fig. 2. Comparison of the pulse duration before and after propagation through the microscopy system: a) autocorrelation and Gaussian fit of the picosecond pulse at the laser output (top) and at the sample plane (bottom), b) reconstructed temporal profile of the pulse at the laser output (black) and at the sample plane (red). TPE fluorescence images of a stained *convallaria majalis* sample obtained at 0.7 mW average power using: c) femtosecond, and d) picosecond pulse trains. Scale bar: 75 μm .

The fluorescence signal depends on the pulse train's duty cycle [4] which is the product of its time duration (τ_p) and f_{rep} . We can achieve a similar result of using the shorter pulses by utilizing longer pulses with a lower f_{rep} , as long as they maintain the same duty cycle [5]. To maintain the same duty cycle, we can change the f_{rep} of the longer pulse train according to:

$$n \sim \frac{p_{\text{avr}}^2}{\tau_p \cdot f_{\text{rep}}} = p_{\text{peak}}^2 \cdot \tau_p \cdot f_{\text{rep}}, \quad (1)$$

where n is the average number of photons emitted by the fluorescence medium per second and p_{avr} and p_{peak} are the average and peak power of the pulse, respectively. The longer pulse can be thought of as a combination of multiple shorter pulses merged. In our case, the f_{rep} of the picosecond pulse train should be equal to 0.3 MHz (picking ratio of 1/50). We have introduced a gradient filter (GF) in front of the microscope to keep the powers at the same levels.

Figures 2(c)-(d) show the results of imaging a *convallaria majalis* root transverse section stained with acridine orange using the pico- and femtosecond pulse trains with 0.3 MHz and 15.23 MHz, respectively. For both images, the p_{avr} was equal to 0.7 mW, and their size was set to 1024x1024 pixels with the dwell time of one pixel set to 10 μs . The image obtained using the femtosecond pulse train is visibly darker. The mean pixel intensity of the image captured using the picosecond pulse train was equal to 0.54 V, compared to 0.25 V for the femtosecond pulse train. This results in a 54% higher fluorescence signal for the longer pulse train. This difference might be caused by the shape of the pulses (as our pulses are not perfectly Gaussian) and the dispersive effects of the microscopy setup (estimated to equal several thousands of fs²) on the shorter pulses which elongate the pulse and lead to the decrease in the p_{peak} . These findings showed that temporal compression of fiber lasers isn't always necessary and can be bypassed by using a more compact and user-friendly all-fiber setup.

In conclusion, we have underscored the benefits of employing multiphoton microscopy with a high-energy Yb: fiber NALM oscillator at a reduced repetition rate (f_{rep}). Our study revealed that the picosecond pulse train delivered superior image quality compared to the femtosecond pulse train, despite ensuring similar duty cycles and the same average powers. This compact, all-fiber system features adjustable f_{rep} through a pulse-picking unit and is user-friendly due to its resistance to chromatic dispersion. These results present a new perspective on multiphoton microscopy and are particularly useful in multiphoton endoscopic applications.

Funding: National Science Centre, Poland (2021/43/D/ST7/01126)

References

- [1] Denk, W., Strickler, J. H., and Webb, W. W., "Two-Photon Laser Scanning Fluorescence Microscopy," *Science* 248, 73–76 (1990).
- [2] König, K., Schenke-Layland, K., Riemann, I., and Stock, U. A., "Multiphoton autofluorescence imaging of intratissue elastic fibers," *Biomaterials* 26, 495–500 (2005).
- [3] Bogusławski, J., Kwaśny, A., Stachowiak, D., and Soboń, G., "Increasing brightness in multiphoton microscopy with a low-repetition-rate, wavelength-tunable femtosecond fiber laser," *Opt. Continuum* 3, 22 (2024).
- [4] Song, J., Kang, J., Kang, U., Nam, H. S., Kim, H. J., Kim, R. H., Kim, J. W., and Yoo, H., "SNR enhanced high-speed two-photon microscopy using a pulse picker and time gating detection," *Sci Rep* 13, 14244 (2023).
- [5] Karpf, S., Eibl, M., Sauer, B., Reinholz, F., Hüttmann, G., and Huber, R., "Two-photon microscopy using fiber-based nanosecond excitation," *Biomed. Opt. Express* 7, 2432 (2016)

Effect of chain length on *skeletonema pseudocostatum* as probed by THz spectroscopy.

R. Mushtaq,¹ C. Gambardella,² R. Miroglio,² F. Novelli,³ D. Paparo,⁴ M. Paturzo,⁴ A. Rubano,¹ A. Sardo⁵

1. Physics Department 'E. Pancini', University of Napoli 'Federico II', Napoli, Italy

2. Institute for the Study of Anthropic Impact and Sustainability in the Marine Environment, National Research Council, Genova, Italy

3. Ruhr University Bochum, DE, Germany

4. Institute for Applied Sciences and Intelligent Systems, National Research Council, Pozzuoli, Italy

5. Marine Biotechnology Department, Zoological Station 'A. Dohrn,' Napoli, Italy

Abstract- Microalgae, particularly diatoms, are well suited for monitoring environmental health, especially in assessing the quality of seas and rivers in terms of organic matter, nutrients, and heavy metal pollution. They respond rapidly to changes in habitat quality. In this study, we focused on *Skeletonema pseudocostatum*, a unicellular alga that forms chains depending on environmental conditions. Specifically, we explored whether metal toxicants could affect the growth of these algal chains, potentially serving as an ecotoxicological indicator of heavy metal pollution. We utilized THz spectroscopy in conjunction with standard optical microscopy to observe the formation of these chains and their response to toxicants. Despite the strong absorption of terahertz radiation in water, we demonstrate that changes in water absorption in the terahertz range due to water-diatom interaction can provide insights into diatom chain length.

Keywords- THz-TDS spectroscopy, diatoms, marine ecotoxicology

I - Introduction

In THz-TDS experiments the THz waveforms $E(t)$ by fast Fourier transform were transformed in the frequency domain to obtain the complex field $\tilde{E}(\nu) = E(\nu)e^{i\varphi(\nu)}$ having the magnitude and the phase information which are directly linked to the complex index of refraction $\tilde{n}(\nu) = n(\nu) + iK(\nu)$, and absorption coefficient $\alpha = 4\pi\nu k/c$. The need for high-sensitivity of THz-TDS lies in the problem of very strong absorption of THz waves in aqueous systems, as in our case, combined with the need of measuring very faint changes of the THz spectrum due to the presence of intoxicated diatoms in the solution. Marine algae are one of the most extensively studied marine organisms, responsible for over 50% of the primary photosynthetic productivity that occurs on Earth each year¹. Ecotoxicological studies have increased significantly in the last decades following an exponential growth in the production and use of chemicals in agriculture, medicine, and in various industrial sectors, leading to an increasing release of toxic contaminants (heavy metal, pharmaceutical product, hydrocarbon, plastic), into rivers and oceanic waters².

II- Materials and method

The THz-TDS consist of input laser source, an amplified titanium sapphire (Ti:Sa) laser emitting ~90 fs long pulses at 790 nm, output power of 7 W at 1 kHz repetition rate producing intense and almost single-cycle THz pulses via optical rectification in lithium niobate. Samples were enclosed in a 0.5 mm thick layer of static sample holder, at stabilised temperature $20 \pm 0.05^\circ \text{C}$. The setup is enclosed in a box, purged with nitrogen to control the relative humidity³. In first set of measurement THz-TDS experiment were recorded on diatoms at different concentrations in a range of (5,10,100,500,850) $\times 10^3$ cells /ml prepared by algal counting, using Bürker chamber method. Secondly, toxicity test had been performed according to the test method ISO 10253. The microalga *s. pseudocostatum* were doped to different $(\text{PbNO}_3)_2$ concentrations (0, 0.5,1,2,4 mg/litter). After 48h and 72 h, the effect in chain length of control sample and dopped ones was evaluated by THz-TDS.

III- Results and discussion

By using the Lambert–Beer Law, difference of diatoms with seawater-based culture medium (SBCM) i.e. F/2 culture medium in term of the refractive index and absorption coefficient can be determined from the ratio of the transmitted intensities of the sample and reference^{4,5}.

$$\Delta n = n_{\text{sample}}(\nu) - n_{\text{ref}}(\nu) = \frac{c}{\nu d} \arg \left(\frac{E_{\text{sample}}(\nu)}{E_{\text{ref}}(\nu)} \right) \quad (1)$$

$$\Delta\alpha = \alpha_{sample}(\nu) - \alpha_{ref}(\nu) = -\frac{1}{d} \ln\left(\frac{E_{sample}(\nu)}{E_{ref}(\nu)}\right) \quad (2)$$

Here $\alpha(\nu)$ is the frequency-dependent absorption coefficient, d is the sample thickness i.e. 0.5mm, $E_{sample}(\nu)$ the transmitted intensity from the sample, and $E_{ref}(\nu)$ the transmitted intensity from the reference channel. Figure 1 representing the absorption spectra at different concentrations. The Effect of toxicant on chain length after 72 hours in term of $\Delta\alpha$ in Figure 2, and numbers of cells in a chain are shown in Figure 3.

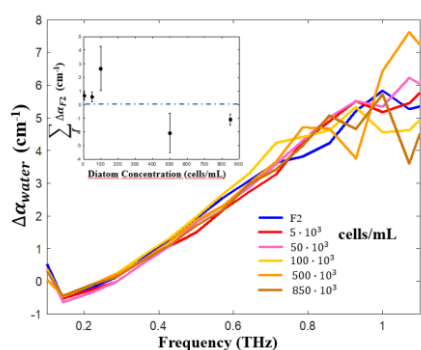


Fig. 1. $\Delta\alpha$ as a function of diatoms at different concentration, number of cells/ml

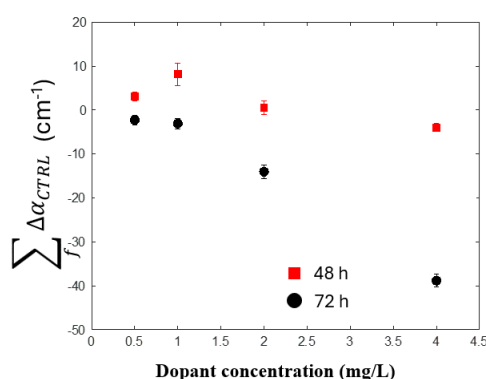


Fig. 2. $\Delta\alpha$ as a function of dopant concentration in comparison to control

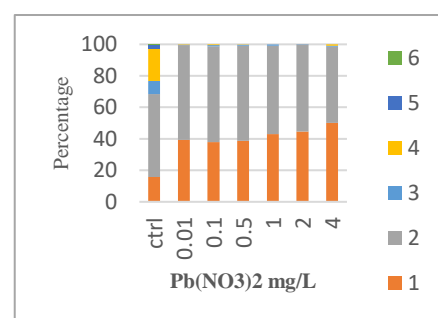


Fig.3. chain length effect of control verses Pb doped diatoms after 72 hours

IV- Conclusion

We utilized THz spectroscopy in conjunction with standard optical microscopy to observe the formation of chains and their response to toxicants. The absorption spectra is not sensitive to the different concentrations of diatoms but it is sensitive with chain length, as gradual decrease can be observed after 72 hours. THz spectroscopy will be very helpful in ecotoxicology as compared to via optical microscope. The sensitivity of THz Spectrophotometer towards diatoms concentration is still unknown and under consideration of our next experiments by using other THz-TDS system with different spectral bandwidth, to find the optimal frequency range to monitor the algal growth.

Acknowledgement

This research is funding by "PON-Research and Innovation Program".

References

- [1] Nagy, S.S., *Collecting, cleaning, mounting, and photographing diatoms*, in *The diatom world*. 2011, Springer. p. 1-18.
- [2] Paixao, Susana M., et al. "Performance of a miniaturized algal bioassay in phytotoxicity screening." *Ecotoxicology* 17 (2008): 165-171..
- [3] et al., *Toxic effect of metal doping on diatoms as probed by Broadband Terahertz Time-Domain Spectroscopy*. *Molecules*, 2022. **27**(18): p. 5897.
- [4] Novelli, Fabio. "Terahertz spectroscopy of thick and diluted water solutions." *Optics Express* 32.7 (2024): 11041-11056.
- [5] Schwaab, Gerhard, Federico Sebastiani, and Martina Havenith. "Ion hydration and ion pairing as probed by THz spectroscopy." *Angewandte Chemie International Edition* 58.10 (2019): 3000-3013.

Femtosecond fiber delivery at 920 and 1050 nm for two-photon microscopy

L.H. Luisa Hofmann¹, A.J. Alexander Jelzow¹, H.S. Helge Schmidt¹

¹ TOPTICA Photonics AG, Lochhamer Schlag 19, D-82166 Graefelfing, Germany.

Abstract

We present femtosecond laser systems at 920 and 1050 nm delivering ultrashort pulses via a hollow-core photonic bandgap fiber (HC-PBGF). The laser system is designed to simplify two-photon microscopy applications and can be used for miniaturized two-photon microscopes. While previously presented solutions have been tailored to a specific length and dispersion coefficient of the HC-PBGF, we now show a compact and flexible scheme for dispersion compensation which is compatible with a wide range of fiber types and lengths.

In addition, this new approach fully maintains the capability of software-controlled dispersion compensation in the range from 0 to $-40,000 \text{ fs}^2$ after the pulse delivery fiber. Hence, the dispersion of common two-photon microscopes can be pre-compensated in order to obtain compressed pulses at the sample plane. Our newly developed system displays excellent long-term fiber coupling stability under varying environmental conditions.

It is capable of polarization-preserving femtosecond pulse delivery at 920 and 1050 nm and reaches Watt-level power after the delivery fiber, making it suitable for in-vivo brain imaging in mouse models.

References

1. Zong, W., Obenaus, H. A., Skytøen, E. R., Eneqvist, H., de Jon, N. L., Vale, R., Jorge, M. R., Moser, M. B., and Moser, E. I., "Large-scale two-photon calcium imaging in freely moving mice," *Cell* 7(185), 1240–1256 (2022).
2. Hellerer, T., Polzer, C., Friedenauer, A., Greisberger, I., Wolfring, B., and Skrobol, C., "920-nm fiber laser delivering 100-fs pulses for nonlinear microscopy," in [Multiphoton Microscopy in the Biomedical Sciences XIX], Periasamy, A., So, P. T. C., and Köhönig, K., eds., 10882, 108820U, International Society for Optics and Photonics, SPIE (2019).

Limitations of effective medium models for water content estimation in the THz frequency range

Sonal Saxena^{1,*}, Ciaran Bench¹, Diksha Garg¹, Patric Boardman¹, Michal Mrnka¹, Harry Penketh¹, Nicholas Stone¹, and Euan Hendry¹

¹Department of Physics and Astronomy, University of Exeter, Exeter, EX4 4QL, UK

*s.saxena@exeter.ac.uk

In recent years, there is a surge of interest in biomedical applications of THz radiation owing to the non-ionising nature of the radiation and the sensitivity to differences in tissue water content in this frequency band. Since there is an established correlation between variations in tissue water content and several pathological conditions such as cancer, it is thought that THz radiation may form the basis of future diagnoses and early-stage detection approaches for such conditions. The exploration of THz optical properties of tissue mimicking materials, where one can controllably change the water content in a sample, is therefore crucial.

In this study, we do exactly this, by investigating the THz optical properties of gelatine hydrogels over a range of hydration levels. A significant fraction of the water content in a biochemical sample has properties that are different to those of pure ('free') water since the molecules adjacent to large biomolecules have restricted mobility - this fraction is typically referred to as 'bound' water. The accepted model for determining the optical properties of a tissue or phantom assumes that only free water varies with hydration level, and therefore a fully dried sample would comprise of bound water exclusively. We compare our results to an effective medium model from the literature that is commonly used to describe both phantoms and real tissues and find large discrepancies between the predicted and measured optical parameters. To better understand the underlying interactions in the phantom which determine the THz optical properties, we also record Raman spectra, and find a bound water concentration which varies continuously with hydration level. This observation lies in distinct contrast to the assumptions which lie behind the effective medium model. It follows that the effective medium model in its simplest form is not applicable for extracting the hydration values from tissues or samples, as per its common application in the literature, and doing so yields errors of up to 50%.

Changes in the Excited State Dynamics of ArchaeRhodopsin-3 via Site-Specific Mutations

Krystyna Herasymenko¹, Arnaud Marquette¹, Masae Konno-Inoue², Michel Sliwa³, Keiichi Inoue², Stefan Haacke¹

¹University of Strasbourg - CNRS, Strasbourg Institute of Material Physics and Chemistry, 23 Rue du Loess, 67000, Strasbourg, France

²The Institute for Solid State Physics, University of Tokyo 5-1-5, Kashiwanoha, Kashiwa, Chiba, 277-8581, Japan

³LASIRE, Université de Lille, CNRS, UMR 8516, 59000, Lille, France
inoue@issp.u-tokyo.ac.jp; stefan.haacke@ipcms.unistra.fr

Abstract Multiple ultrafast spectroscopy techniques are employed to investigate the excited-state dynamics of ArchaeRhodopsin-3, a genetically encoded voltage indicator. As a result of site-specific mutations, a 100-fold increase in fluorescence lifetime is observed.

1. Introduction

ArchaeRhodopsin-3 (AR-3) is a light-driven proton pump found in *Halorubrum sodomense*. AR-3 was reported to display a low, but detectable fluorescence, which, when integrated in membranes of live cells, was shown to depend strongly on the membrane potential [1]. AR-3 then was developed for voltage imaging of mammalian neurons. In recent years, improvements in rhodopsin-based sensors have mainly stemmed from mutations in AR-3, yielding improved indicators with fluorescence quantum yields (FQY) reaching up to 1.2% like QuasAr 1 to 3, NovArch and Archon 1 and 2 [2,3]. Understanding the effect of the mutations is essential for the future development of rhodopsin-based fluorescent and voltage-sensitive transmembrane sensors. Recently, quantum chemical simulations have shown a correlation between the computed excited state barrier and experimentally determined FQY of the numerous AR-3 mutants. Unlike other retinal proteins, this barrier is predicted to arise from the mixing of the ground and excited states [4].

This work is focused on the detailed investigation of the effects of mutations of residues located in the protein cavity, and which modify the electrostatic interactions with the protonated retinal Schiff base chromophore. For this study, we used the wild-type AR-3 protein and its double mutant DETC and the quintuple mutant ARCH 5[2] at pH 6. All proteins were expressed in *Escherichia coli* cells and purified.

2. Results

2.1. Excited state dynamics

To investigate the mutation's impact on excited-state dynamics, Fluorescence Up-Conversion Spectroscopy (FLUPS) with 120 fs time resolution and 580 nm excitation pulses was employed. Figure 1 Panel A presents the experimental normalized kinetic traces at the fluorescence peak (dots) for WT AR-3 (orange) and its mutants DETC (green) and ARCH 5 (violet). The results clearly show that the WT fluorescence decays in a few ps and the mutants' fluorescence lives significantly longer. The kinetics have a bi-exponential decay character for all of the samples. Solid lines display the results of the two-exponential fit, yielding average fluorescence lifetimes of 0.5 ps, 30 ps, and 66 ps for WT, DETC, and ARCH-5, respectively. These are in quantitative agreement with the relative increase of the FQY of the mutant with respect to wt-AR-3.

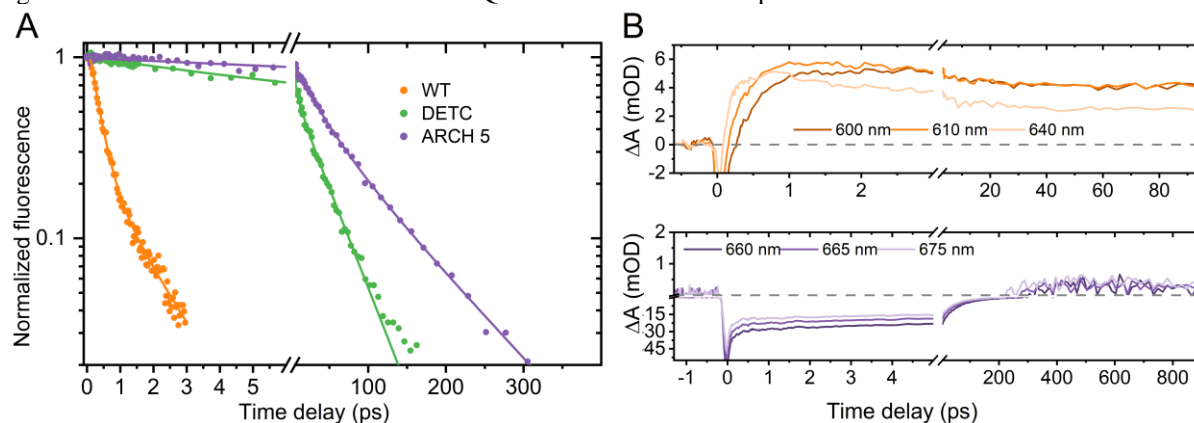


Fig. 1. Ultrafast spectroscopy results. (A) FLUPS: Comparison of the normalized fluorescence kinetics at the maximum of emission of WT AR-3 and its mutants. Dots represent experimental data and lines result of two-exponential fit (B) TAS: Comparison of the transient absorption kinetics of photoproduct formation (positive signal) in WT (top) and ARCH 5 (bottom) at the wavelength listed in the legend.

In addition, Transient Absorption Spectroscopy (TAS) experiments in the 400-1000 nm spectral range with 60 fs time resolution were conducted to confirm the excited state lifetimes of each of the samples. Moreover, we estimate the isomerization quantum yield (IQY) comparing the intensity of the photoproduct absorption after its formation (Figure 1 Panel B: positive signal at 1 ps for WT and 500 ps for ARCH 5). We observed that mutation causes more than a 50-fold decrease of IQY in the ARCH-5 compared to the WT. This indicates that the excited state barrier in Arch-5 largely reduces IQY, and suggests that the 66 ps lifetime is limited by internal conversion rather than isomerization.

3. Conclusion

Our ultrafast experiments offer valuable insights into the impact of mutations on the excited state dynamics of the membrane voltage sensor AR-3. The studied mutants exhibit prolonged excited state lifetimes (66 ps for ARCH 5 compared to 0.5 ps for WT) characterized by a biphasic decay, with the average fluorescence lifetimes directly proportional to the FQY. Throughout this extended excited state duration, the majority of molecules revert to the original ground state, while only a minimal fraction (appr. 2% for ARCH 5) undergo isomerization. Moreover, the vibrational and torsional modes of the excited state demonstrate the effect of the excited state barrier on the twisting dynamics of the retinal molecule. Combining the obtained experimental results with numerical calculation of the vibrational modes will allow us to evidence the effect of mutations on modifying the excited state potential energy surface, and possibly identify the pathway of ps internal conversion without isomerization.

[1] J. M. Kralj et al, "Optical recording of action potentials in mammalian neurons using a microbial rhodopsin," Nat. Methods 9, 90–95 (2011).

[2] R. Scott McIsaac et al, "Directed evolution of a far-red fluorescent rhodopsin," PNAS, 111, 13034-13039 (2014).

[3] Bando et al. "Genetic voltage indicators," BMC Biol., 17 (2019).

[4] L. Barneschi et al, "On the fluorescence enhancement of arch neuronal optogenetic reporters," Nat Commun, 13, 6432 (2022).

[5] S. O. Smith et al, "Vibrational analysis of the *13-cis*-retinal chromophore in dark-adapted bacteriorhodopsin," J. Phys. Chem., 91, 804-819 (1987).

Imaging in lossy media via complex wavevectors

Abstract— The use of complex wave-vector in recent phenomena of spin-momentum locking inspired us to investigate a method of achieving improved transmission of light across optically opaque materials, solving the Helmholtz equation for complex values, via introducing a passive metasurface with a varying transmission phase and amplitude simultaneously, with interesting applications in acoustics structures, telecommunications bandwidth transmission or biophotonics for exotic beam shaping for analyzing and treating malignant cells subcutaneously without damaging the skin.

Keywords— *Polarization-loss locking, near-field photonics, lossy propagation, Bullseye metasurface, passive metasurface,*

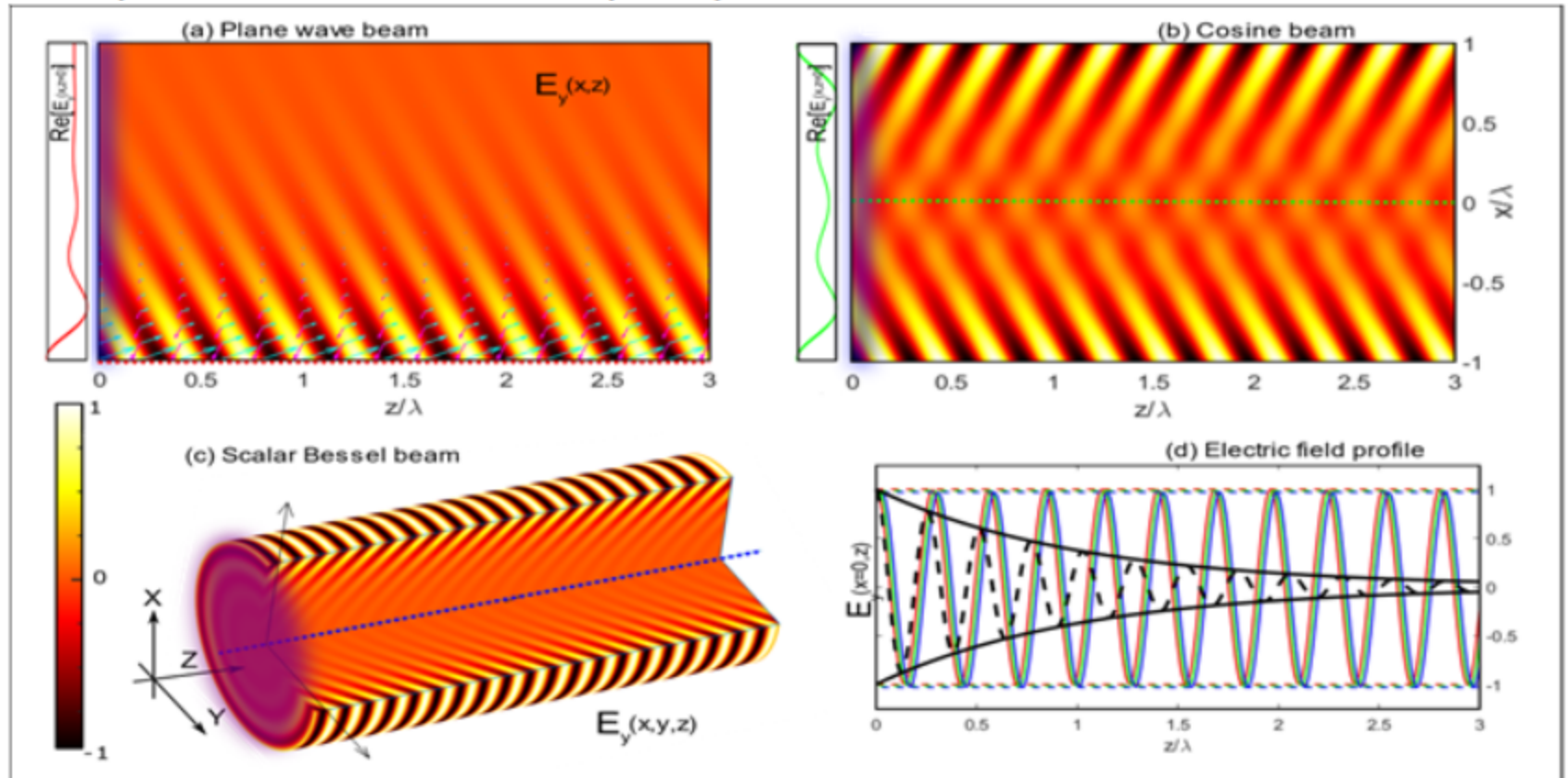
I. INTRODUCTION

The study of propagation of electromagnetic waves inside classically forbidden structures has been currently developed

in Bragg media [1], evanescent waves [2] or lossy materials [3-4] via clever engineering of the incident waves, obtaining an extraordinary transmission in isotropic materials with refractive index $n=n'+in''$, with non-trivial imaginary part, causing in principle (via Helmholtz equation) a complex transmitted wavevector with an unavoidable exponential attenuation in the penetration direction (here z) by Beer-Lambert law.

Studying the constraints derived from Maxwell's equations it is possible to obtain the exact solution of the incident wavevector (here, k_x) for a purely harmonic oscillation inside the lossy material (corresponding to a real k_z). Both are linked to background wavenumber k_0 via the dispersion relation:

$$k_z = [(nk_0)^2 - k_x^2]^{1/2} \quad (1)$$



Electric field transmission for: ideal plane wave (a, red), cosine (b, green), and Bessel beam (c, blue) through a lossy material by placing an infinite meta-surface at $z=0$ that introduces an spatially-dependant complex gradient ($\Delta k_x, \Delta k_y$), showing constant amplitude (d) in comparison with the original case (black).

II. RESULTS

Here we propose a general method for achieving perfect ideal transmission with (almost) any arbitrary incident beam.

This is performed by introducing a flat designed structure, a metasurface, that introduces an additional wavevector gradient. In the case of the phase, it was performed in [5] for a generalisation of Snell's law of refraction, but here we also

introduce a simultaneous intensity control, in such way the effective incident wave is $k_x^i + \Delta k_x$, as a spatially-dependent gradient for the transmitted wavevector, in general complex. Solving the system, we observe that for a purely real wavenumber k_z , we need to satisfy two complementary constraint: which can be encapsulated in the following equation:

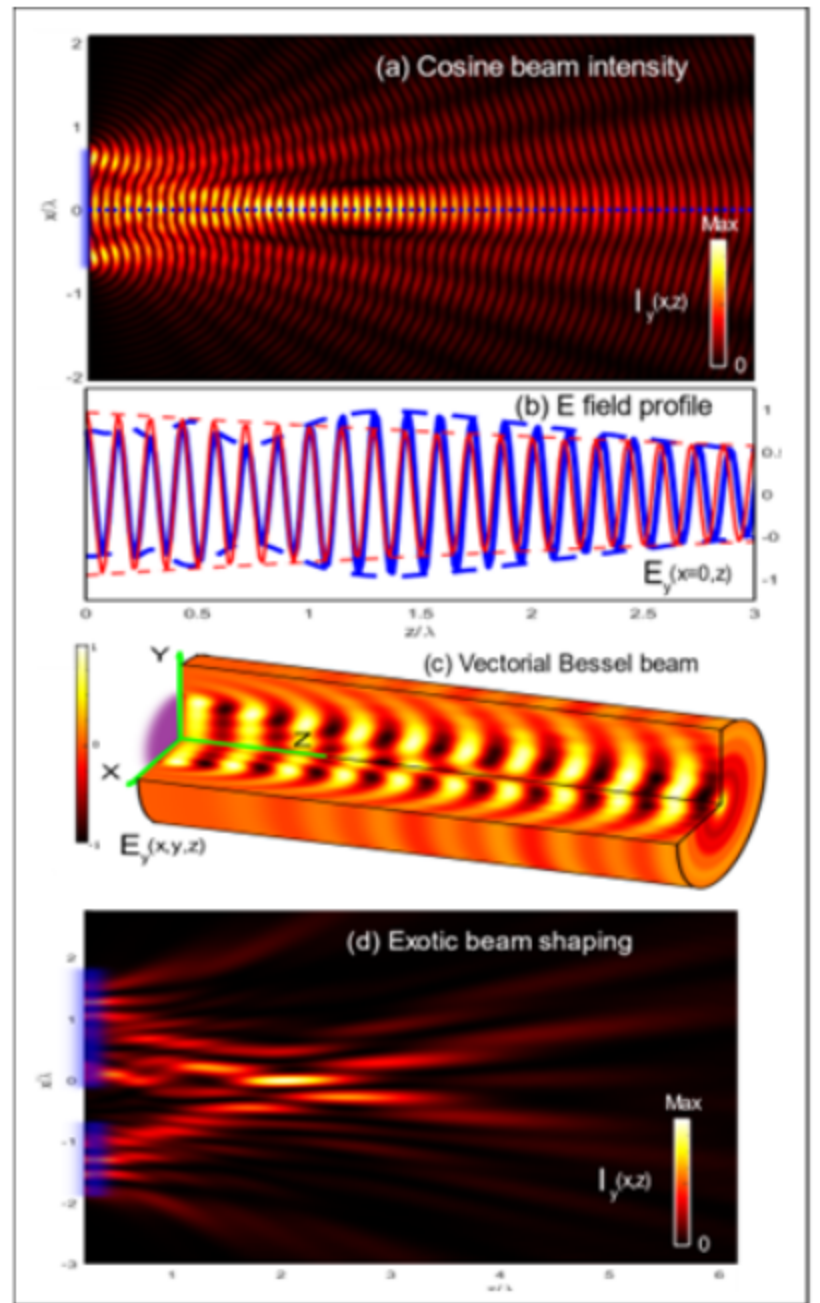
$$k_x = k_0 (fn' + ifn'') \text{ for any } 0 < f < 1 \quad (2)$$

being f the internal degree of freedom conserved from the phase control. From here, we can see the implementation of this design in Fig.1, where we can observe a infinite transmission inside the material for different kinds of incident initial beams (on the left of subfigures a,b) from a single exponential, opposite exponential and a full ring of them, while in all cases, the intensity don't change along the centrosymmetric region (d), thanks to the infinite metasurface (in light purple).

Nevertheless, the trade-off is that the above condition would require an increasing monotone complex value of k_x associated with an exponential decay (and increase) in the amplitude of the transmission along the direction parallel to the interface, requiring an infinite energy to maintain the propagated beam. Therefore, to avoid this unphysical infinite amplitude when moving away from the centre of the beam, we can window the initial excitation maintaining the intensity as far as possible thank to locality of Maxwell equations. This latter case is presented in Fig. 2, where a cosine beam (a) has been windowed obtaining a *bullseye metasurface* intensity profile, where in $x=0$, we still observe an increase in the transmission depth (b); and were the cylindrical full Bessel beam case (c) is also included, observing the anomalous transmission inside the lossy material.

III. DISCUSSION

Here we have proposed how placing a passive bullseye metasurface, it is possible to create exotic transmitted beams inside complex media, to allow practical applications, like medical imaging, or focusing of light into a specific tuneable point inside the medium, without over-heating the boundaries in the interface, as can be seen in Fig.3(d), where we have the more intensity inside than in the start. Another branch of applications relies on the increase of intensity obtained. We can design specific bullseye metasurfaces such that the peak of them corresponds to the total length of an (dispersive) object to surpass, increasing the transmitted intensity, which could be used in buildings for increasing the telecommunication wireless coverage or based on electromagnetic-acoustic similarities, an acoustic counterpart could be developed, for instance to improve detection techniques or in acoustic isolation for walls. Via this inductive approach to a classic problem, by allowing complex numbers rather than real in dispersion relation, in analogy with [6]. We aim that this inductive technique could lead to allow new nuances and corollaries in Physics.



Bullseye metasurface proposal: a finite meta-surface at $z=0$: Intensity of the electric field transmission for a cosine beam (a), field profile along the centre of the beam (b) -blue- in comparison with the case without metasurface -red-, vectorial Bessel beam (c) field distribution and through a lossy material. In (d) a four mode beam is used to obtain a hotspot inside the lossy material, while the region close to $x=0$ has a lower intensity, which can be potentially used for plasmonic, biomedical imaging and techniques or optical trapping.

REFERENCES

- [1] A. Yulaev, S. Kim, Q. Li, D. A. Westly, B. J. Roxworthy, K. Srinivasan, and V. A. Aksyuk, (2021). J. Clerk Maxwell, A Treatise on Electricity and Magnetism, 3rd ed., vol. 2. Oxford: Clarendon, 1892, pp.68–73.
- [2] H. Li, A. Mekawy, and A. Alù, Phys. Rev.Letters 127, 014301 (2021).
- [3] F. Frezza and N. Tedeschi, Optics Letters 37, 2616 (2012).
- [4] P. Baccarelli, F. Frezza, P. Simeoni, and N. Tedeschi, Materials 11, 1595 (2018).
- [5] N. Yu, P. Genevet, M. A. Kats, F. Aieta, J.-P. Tetienne, F. Capasso, and Z. Gaburro, Science 334, 333 (2011).
- [6] S. Perea-Puente, F. J. Rodríguez- Fortuño, Phys. Rev. B 104, 085417 (2021)

Spectro-temporal mapping in broadband sum-frequency generation infrared spectroscopy

Wolfgang Lakata, Christoph Leithold, Cristina Consani and Gerald Auböck

Photonic Systems, Silicon Austria Labs GmbH, Europastrasse 12, 9524, Villach, Austria

Sum-frequency generation infrared (SFG-IR) spectroscopy became a versatile tool for surface and interface science. Its intrinsic surface/interface selectivity combined with its high sensitivity enable numerous scientifically and technically relevant investigations not addressable by other spectroscopic means, and among others, most relevant for bio sciences.

Here we present our recently implemented femtosecond (fs) SFG-IR setup, operating at a high repetition rate of 40 kHz and allowing for broad band spectroscopy through a tuning range from 2 to 12 μm . A frequent problem for fs SFG-IR spectroscopies is the non-resonant background signal generated from many substrates masking and, due to interference, distorting, the resonant spectrum of interest. We address this by implementing the generation of time asymmetric visible pulses with a sharp rising and slowly decaying slope, respectively, by means of a custom designed etalon filter [1]. This allows to avoid temporal overlap of the VIS and IR pulse on the sample, thus eliminating non-resonant contributions, while still providing sufficient temporal overlap between the coherence generated in the target molecules by the IR pulse and the visible pulse to obtain well resolved SFG spectra [2].

Beyond this, the excellent signal to noise ratio of our setup allows us to investigate the evolution of the SFG signal as function of the time delay between the IR and VIS pulse, respectively, in very reasonable measurement times. Such data is shown for SFG spectra of PMMA spin coated on a gold surface in figure 1.

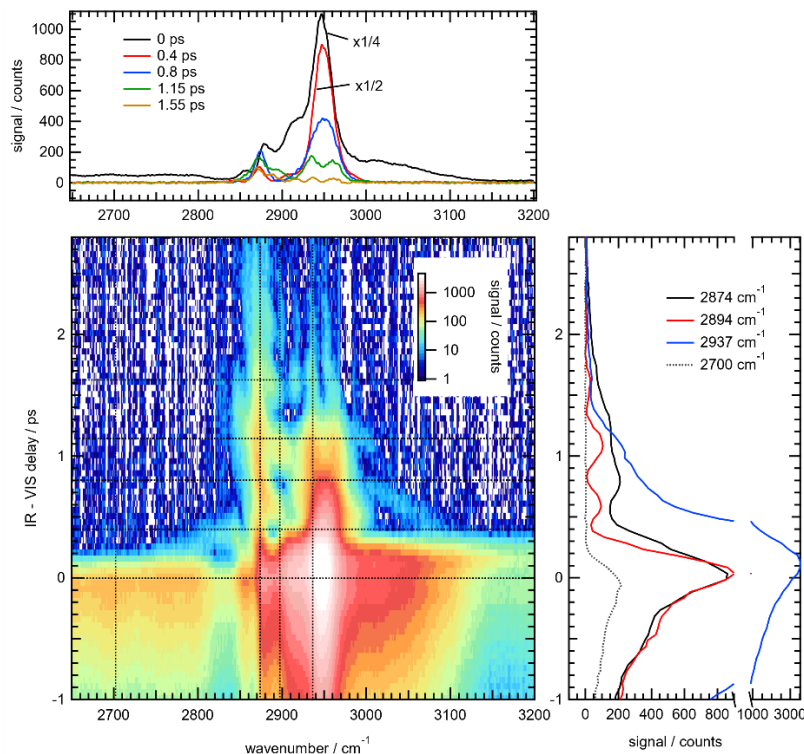


Figure 1: SFG-IR spectrum of PMMA on a gold surface. The acquisition time was one second per spectrum. A 2D map is shown in the center, note that the color scale is logarithmic to enhance visibilities of the smaller features at positive IR – VIS delay times. The upper panel shows spectra at different delays and the right panel time traces at different spectral positions, respectively. Their position is indicated by horizontal and vertical lines in the 2D map.

For zero and negative delays (where IR and VIS pulse overlap on the sample) high resonant signals stemming from the various CH stretching modes and some non-resonant contribution is visible. Its time dependence mainly reflects the temporal intensity profile of the VIS pulse. For positive delays non resonant contributions vanish and we see a rapid reduction of the resonant signal with a rather complex spectro-temporal evolution (see fig.1).

Looking at spectra at different delays, it is apparent, that spectrally broad features decay rapidly revealing the presence of weaker, spectrally narrower lines at large delays. This is straight forward to understand qualitatively. In our experiment the sharp onset of the VIS pulse probes the time-evolution of the vibrational polarization introduced by the IR [2]. Thus, spectrally broad features, which correspond to short coherence times, disappear faster while narrower features remain present at relatively large delay time.

Simultaneously, beatings are observed as a function of delay time at various spectral positions. These originate from interference between resonant SFG signals generated from different vibrational lines and reflect the spectral spacing between them. We note that these observed oscillations in general also yield (relative) phase information and can thus provide additional information on the (relative) orientation of vibrational modes contributing to the interference.

A closely related spectral narrowing effect for SFG spectroscopy using IR/VIS delay, though in a different configuration using tune-able ps IR pulses, was found and is discussed in detail in ref. [2]. It can in general be seen as a special case of spectral line-narrowing by introducing a delay between excitation and observation [3]. To our knowledge, however, we report the first observation of this effect in fs broadband SFG-IR spectroscopy.

The method demonstrated here can be used to reveal detail within spectrally congested regions (like the CH region for non-small molecules) or may be used to detect subsets of molecules, which are in a more ordered configuration (and thus show narrower linewidth), within complex samples.

[1] A. Lagutchev, S. A. Hambir and D. D. Dlott, *J. Phys. Chem. C* 2007, 111, 37, 13645–13647 (2003)

[2] S. Roke, A. W. Kleyn, M. Bonn, *Chem. Phys. Let.* 370, 1-2, 227-233 (2003)

[3] W. Zinth, M.C. Nuss, W. Kaiser, *Opt. Comm.* 44, 4, 262-266 (1983)

Multiphoton frequency-domain fluorescence lifetime imaging microscopy using digital homodyning

Jakub Boguslawski[#], Łukasz Sterczewski, Katarzyna Kunio, Grzegorz Soboń

Laser & Fiber Electronics Group, Faculty of Electronics, Photonics and Microsystems,
Wrocław University of Science and Technology, Wybrzeże Wyspiańskiego 27, 50-370 Wrocław, Poland
[#]corresponding author email: jakub.boguslawski@pwr.edu.pl

Multiphoton microscopy [1] is an advanced imaging technique that uses multiple lower-energy photons to excite fluorophores. This approach allows for deeper tissue imaging and reduces photodamage compared to conventional fluorescence microscopy. By leveraging nonlinear optical processes, it provides detailed visualization of cellular structures in intact biological samples. Two-photon excited fluorescence is the most commonly used modality. In its classical variant, it provides information about the intensity of the fluorescence, and hence, about the structure of the sample. Fluorescence lifetime imaging microscopy (FLIM) is an imaging technique that measures the decay time of fluorescence from a sample to provide contrast based on the lifetime of fluorescent molecules rather than their intensity [2]. It is used for analyzing the biochemical environment of cells, including interactions, local pH, and molecular binding, offering insights into cellular functions and dynamics. FLIM techniques can be generally classified into two groups: time- and frequency domain. On one hand, time-domain techniques are very precise, but sophisticated, slow, and require advanced and costly equipment. On the other hand, recent results show that frequency-domain techniques can be much faster, and sufficiently precise, and are starting to gain attention in the scientific community [3]. Here, we show that multiphoton frequency-domain FLIM (FD-FLIM) can be easily realized using commonly available lock-in amplifiers. Lifetime information can be obtained through simple matrix operations and displayed in real time.

Figure 1 shows the schematic of our experimental multiphoton microscopy setup. A custom-built Yb: fiber oscillator was used as the excitation source (described in detail in [4]). The laser provided 205 fs pulses, 15.23 MHz repetition rate (f_{rep}), and 1026 nm central wavelength. A gradient index filter (GF) at the entrance of the microscope allowed the adjustment of the laser power incident to the sample. Imaging was performed using a home-built multiphoton microscope system, described in detail in [5]. The system allowed for the detection of two-photon excited fluorescence in epi geometry. As a test sample, a convallaria majalis root transverse section was used. The sample was stained with an acridine orange, a nucleic acid-specific fluorophore. The average power of 14 mW was incident to the sample. Emitted fluorescence light was recorded using a photomultiplier tube (PMT, Thorlabs PMT2102).

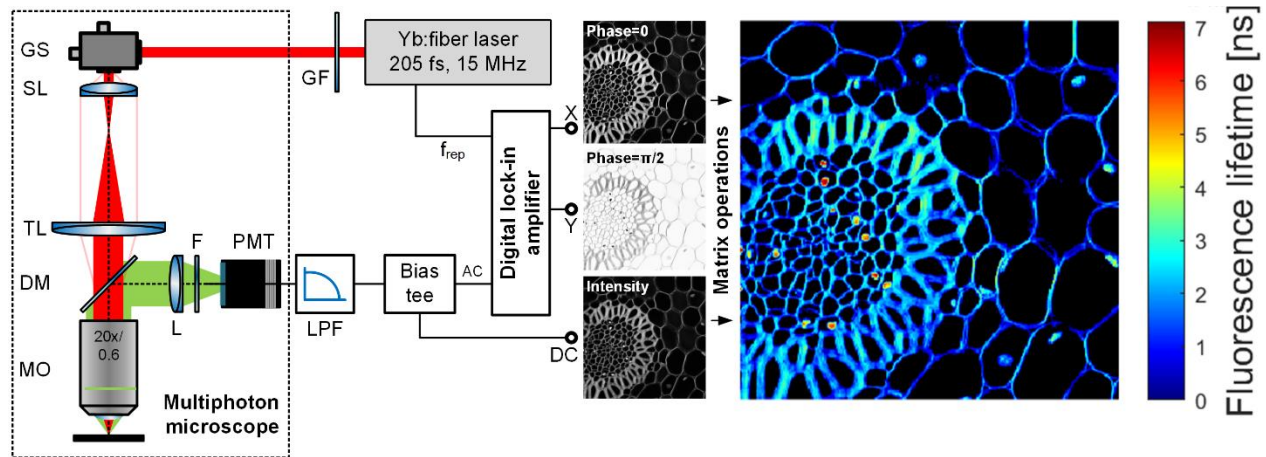


Fig. 1. Schematic diagram of the experimental setup. GF – gradient-index filters, GS – galvanometer dual-axis scanners, SL – scan lens, TL – tube lens, DM – dichroic mirror, MO – 20X microscope objective, L – focusing lens, LPF – RF low-pass filter (21 MHz).

Homodyne detection of fluorescence signal was done using a digital lock-in amplifier (Zurich Instruments HF2LI). First, our laser provided a frequency reference signal that was detected using a phase-locked loop (PLL) in the lock-in amplifier. This frequency was used to generate cosine (phase = 0) and sine (phase = $\pi/2$) harmonic signals for homodyne detection. The output of the PMT was filtered using a 21 MHz low-pass filter to extract the fundamental harmonic of the fluorescence signal. Next, a bias tee is used to divide the AC and DC components of this signal. The DC component can be readily used to reconstruct a typical intensity-based fluorescence image. The AC component

was fed to the input of the lock-in amplifier, multiplied with cosine (X component) and sine (Y component) harmonic signals, low-pass filtered (80 kHz), and provided to the outputs of the lock-in amplifier. The DC output of the bias tee and two outputs of the lock-in amplifier (X, Y) are simultaneously digitized using a data acquisition card (NI PCIe-6363).

The X (phase = 0) and Y (phase = $\pi/2$), and intensity-based images are shown in Fig. 1. A phase lifetime image can be obtained by simple matrix operations on X and Y images, following the equation [6]:

$$\tau = \frac{1}{\omega} \cdot \frac{Y}{X} = \frac{1}{2\pi f_{rep}} \cdot \frac{Y}{X'}$$

where $\omega = 2\pi f_{rep}$. Such calculations can be easily performed in real time using standard PCs. The result of this transformation is displayed in Fig. 1 (right-hand side). Obtained lifetimes are in agreement with previously published results, being within the 1.5 – 3 ns range for cortex structures [7].

In conclusion, we have demonstrated the feasibility of performing a fast, multiphoton FD-FLIM using a typical lock-in amplifier and simple matrix operations. Our results will contribute to the wider dissemination of FLIM techniques, which are usually very technically and computationally demanding.

Funding: National Science Centre, Poland (2021/43/D/ST7/01126).

References

- [1] Denk, W., Strickler, J. H., and Webb, W.W., "Two-Photon Laser Scanning Fluorescence Microscopy," *Science* **248**, 73–76 (1990).
- [2] Peter, M., Ameer-Beg, S. M., "Imaging molecular interactions by multiphoton FLIM," *Biology of the Cell*, **96**(3), 231-236 (2004).
- [3] Zhang, Y., Guldner, I., Nichols, E., Benirschke, D., Smith, C., Zhang, S., and Howard, S., "Instant FLIM enables 4D in vivo lifetime imaging of intact and injured zebrafish and mouse brains," *Optica* **8**(6), 885-897 (2021).
- [4] Kunio, K., Bogusławski, J., and Soboń, G., "Efficient multiphoton microscopy with picosecond laser pulses," *Optics Letters* **49**(16), (2024).
- [5] Bogusławski, J., Kwaśny, A., Stachowiak, D., and Soboń, G., "Increasing brightness in multiphoton microscopy with a low-repetition-rate, wavelength-tunable femtosecond fiber laser," *Opt. Continuum* **3**, 22 (2024).
- [6] Lin, Y., and Gmitro, A. F., "Statistical analysis and optimization of frequency-domain fluorescence lifetime imaging microscopy using homodyne lock-in detection," *J. Opt. Soc. Am. A* **27**, 1145 (2010).
- [7] Bowman, A., Klopfer B., Juffmann, B., and Kasevich, M., "Electro-optic imaging enables efficient wide-field fluorescence lifetime microscopy," *Nature Communications* **10**, 4561 (2019).

Few-cycle ultra-broadband laser microscopy for bioimaging

Christian Maibohm¹, Maria Leonor Ribeiro¹, Tiago Magalhães^{1,3}, Miguel Miranda², Paulo T Guerreiro², Rosa Romero², Helder Crespo^{2,3}, Jana B Nieder¹

1. INL - International Iberian Nanotechnology Laboratory, Ultrafast Bio- and Nanophotonics group, Mestre Jose Veiga s/a, 4715-330 Braga, Portugal
2. Sphere Ultrafast Photonics, Rua do Campo Alegre, 4169-007 Porto, Portugal
3. Instituto de Física de Materiais Avançados, Nanotecnologia e Fotónica (IFIMUP), Departamento de Física e Astronomia, Faculdade de Ciências, Universidade do Porto, Rua do Campo Alegre s/n, 4169 007 Porto, Portugal

Abstract:

Multi-photon microscopy have long been a cornerstone in bio-imaging due to its infrared driven deep tissue penetration, reduced scattering and lowered photo-toxicity. Normal imaging strategy for complex samples with spectrally well separated chromophores using relatively narrow wavelength band fs laser system is to either employ multiple excitation source at the same time or spectrally tune a laser source and do multiple scans.

Here we demonstrate the patented SyncRGB-FLIM (synchronous red-green-blue-fluorescence lifetime imaging microscopy) method where the use of a few-cycle ultra-broadband sub 10 fs laser source provides another path for multicolour nonlinear imaging in a single channel detection geometry, when employing a time-resolved fluorescence detection scheme [1,2]. In the method for optimal performance the few-cycle laser was characterized at the focus using state-of-the-art d-scan technology and is capable of delivering ultrashort laser pulses reaching down to sub-10 fs at the focus of the objective, i.e. at the sample plane.

The SyncRGB-FLIM multicolour bio-imaging technique is capable of efficiently excite multiple chromophores over a >400 nm two-photon absorption range and combined with time-correlated single-photon counting (TCSPC) detection, to record two-photon fluorescence lifetime imaging microscopy (FLIM) images, identify the localization of different chromophores in the cell based on their fluorescence decay properties, as seen in Fig. 1.

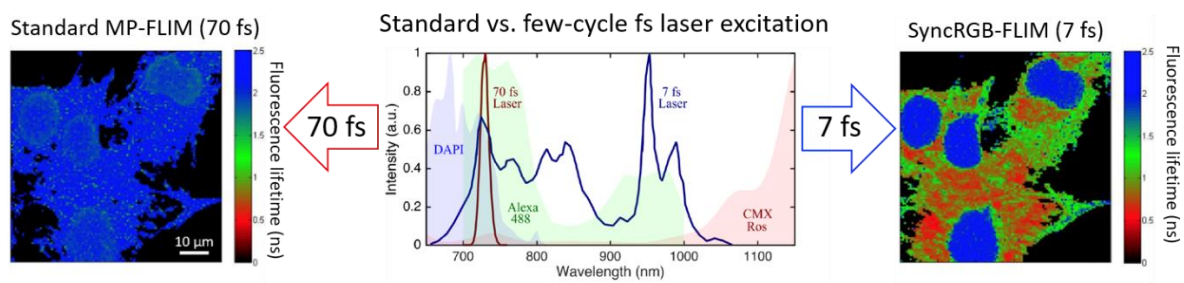


Figure 1: Fig. 1 Single scan excitation efficiency comparison on a multi-chromophore sample (FluoCells#1, DAPI, Alexafluor488 and Mitotracker Red) of a standard at focus optimized 70 fs laser source @730 nm, and a sub-10 fs few-cycle laser source

The SyncRGB-FLIM method was further shown to be able to simultaneous excitation of endogenous markers (NADH/NADPH) in both 2D and 3D cell models including tracking the associated metabolic change as a response to a therapeutic drug, as seen in Fig. 2. The results allow us to confirm a biological response related to the therapeutic action and shows that the SyncRGB-FLIM method is advantageous for nanomedicine research.

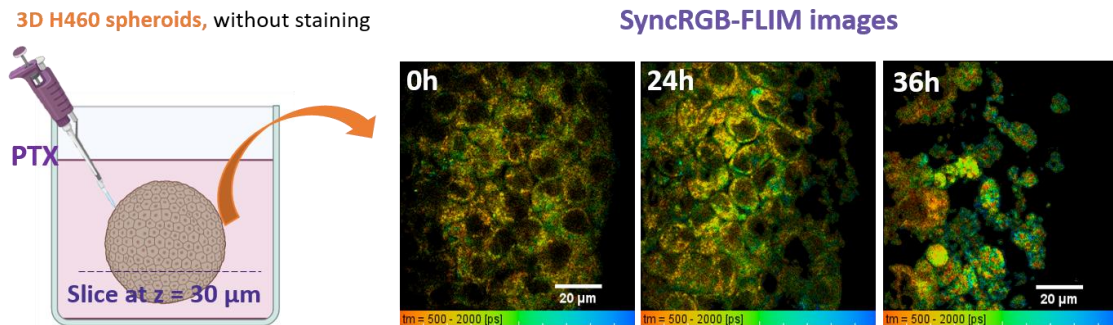


Figure 2: Therapeutic study based on metabolic images via the SyncRGB-FLIM method of A460 3D spheroids exposed to paclitaxel (PTX).

References

[1] Christian Maibohm, Francisco Silva, Edite Figueiras, Paulo T. Guerreiro, Marina Brito, Rosa Romero, Helder Crespo, and Jana B. Nieder, "SyncRGB-FLIM: synchronous fluorescence imaging of red, green and blue dyes enabled by ultra-broadband few-cycle laser excitation and fluorescence lifetime detection," *Biomed. Opt. Express* 10, 1891-1904 (2019)

[2] The EU application number is EP 19724610.1 and US the application number is EP 17047249 both with the title METHOD AND APPARATUS FOR SIMULTANEOUS NONLINEAR EXCITATION AND DETECTION OF DIFFERENT CHROMOPHORES ACROSS A WIDE SPECTRAL RANGE USING ULTRA-BROADBAND LIGHT PULSES AND TIME-RESOLVED DETECTION

Acknowledgement

This research is funded by ANI via the ExtreMED project #NORTE-01-0247-FEDER-045932.

Nanoscale structure and compositional imaging of bacteria with tabletop EUV ptychography

Chang Liu^{(1,2,3)*}, Leona Licht^(1,2,3), Wilhelm Eschen^(1,2,3), Christina Wichmann^(4,5,6), Christian Eggeling^(4,5,6), Jens Limpert^(1,2,3,7) and Jan Rothhardt^(1,2,3,7)

¹Helmholtz Institute Jena, Fröbelstieg 3, 07743 Jena, Germany

²Institute of Applied Physics, Abbe Center of Photonics, Friedrich-Schiller-University Jena, Albert-Einstein-Straße 15, 07745 Jena, Germany

³GSI Helmholtzzentrum für Schwerionenforschung, Planckstraße 1, 64291 Darmstadt, Germany

⁴Institute of Applied Optics and Biophysics, Friedrich Schiller University Jena, Philosophenweg 7, Jena, Germany

⁵Leibniz Institute of Photonic Technology (Leibniz-IPHT), Albert-Einstein-Straße 9, Jena, Germany

⁶Cluster of Excellence Balance of the Microverse, Friedrich Schiller University Jena, Jena, Germany

⁷Fraunhofer Institute for Applied Optics and Precision Engineering, Albert-Einstein-Str. 7, 07745 Jena,

Corresponding Author: liu.chang@uni-jena.de

Abstract: We report on the latest EUV imaging results on Gram-negative and Gram-positive bacteria. The retrieved amplitude and phase images achieve a resolution of 44 nm with excellent material contrast, enabling quantitative investigation of bacterial internal structures and sporulation.

1. Introduction

High-resolution bio-imaging is essential for advancing the comprehension of microbiological structures and composition, playing a crucial role in pharmaceuticals, medicine, and biological research. Microscopy using extreme ultraviolet (EUV) light presents a range of unused potentials in this field [1], complementing electron microscopy and fluorescence microscopy. In addition to its nanometer-scale resolution, it offers high absorption and phase contrast, and greater (μm -scale) penetration depths compared to electron microscopy. Furthermore, EUV radiation enables excellent material specificity from various elemental absorption edges located herein [2]. This allows detailed investigation of cellular and subcellular features in microorganisms.

Recent advances in coherent tabletop EUV sources driven by high harmonic generation (HHG) have significantly enhanced the impact of coherent diffraction imaging (CDI) in this spectral region. Unlike lens-based imaging techniques, CDI avoids losses of imaging optics and avoids aberrations, both being common issues in the EUV. Ptychography [3], a scanning version of CDI, records a sequence of diffraction patterns from overlapping illumination on extended objects and computationally retrieves both the amplitude and phase of the object transmission functions. This quantitative information allows the nanoscale investigation of the material composition of objects without labeling. The capability of EUV ptychography has been demonstrated on biological samples like mouse hippocampal neurons [4], fungi, and bacteria [5], achieving material-specific imaging with sub-60 nm resolution.

Here, HHG-based EUV ptychographic imaging is for the first time applied to study Gram-negative and Gram-positive bacteria. With our home-built high-resolution, high-speed, large-field-of-view ptychographic microscope at 13.5 nm [6] (92 eV photon energy), two species of rod-shaped bacteria, namely *Escherichia coli* (*E. coli*) and *Bacillus subtilis* (*B. subtilis*) were imaged with sub-50 nm resolution and excellent material contrast. Chemical compositions have been gained by scattering quotient analysis, facilitating bacterial identification. Despite their similar size, the two species exhibit distinct differences in chemical composition maps, primarily discerned using the Gram stain method [7]. Additionally, physiological dynamics in *B. subtilis* are observed, including various growth phases and sporulation processes.

2. Experimental setup and results

Our table-top lensless microscope at 13.5 nm (92 eV) employs a high harmonic generation source as depicted in Fig. 1a). The few-cycle laser pulses are focused into a gas nozzle where the EUV photons are generated with a flux of 7×10^9 phot/s/eV at 13.5 nm [8]. A spiral amplitude mask is placed in front of the sample to structure the illuminating beam, resulting in improved image quality [9]. Both mask and sample are mounted on 3D positioners with active interferometric stabilization, facilitating long-time ptychography scans. The measured diffraction patterns are reconstructed by the PtyLab framework [10]. More details on the setup can be found in [11].

In this study, we investigate *E. coli* and *B. subtilis* using our EUV ptychographic microscope. A collection of complex transmission images of both bacterial clusters is presented in Fig. 1b). The EUV images exhibit high absorption- and phase contrast and demonstrate the large penetration depths at this wavelength. It can be observed that *E. coli* and *B. subtilis* share very similar shapes and sizes. Additionally, *B. subtilis* displays physiological dynamics at different growth phases, evident from the variations in transmission and phase shift. For further analysis,

the reconstructed amplitude and unwrapped phase of the EUV images were used to calculate the scattering quotient (f_q). The scattering quotient reveals the composition of the specimens averaged along the propagation direction in each pixel of the image irrespective of sample thickness. The cell wall is visible in both bacteria. Notably, *E. coli* ($f_q \sim 4.08$) possesses a statistically significant higher averaged scattering quotient than *B. subtilis* ($f_q \sim 3.67$), which can be attributed to the compositional differences in the cell walls between Gram-negative and Gram-positive bacteria.

Next, as a spore-forming bacteria, *B. subtilis* was treated with 10 mg/L $MnSO_4$ to create environmental stress [12]. The production of spores, which protect genetic information and enable the bacteria to withstand adverse conditions, was investigated. Fig. 1 c shows the reconstructed complex image containing two cells undergoing sporulation. The endospores exhibit significantly higher scattering density compared to the mother cells, while the mother cells show a reduction in material density. The Fourier ring correlation of the image indicates a diffraction-limited spatial resolution of 44 nm.

In conclusion, we develop a high-performance table-top EUV ptychographic microscope, offering unique capabilities in high-resolution, chemical-sensitive biological imaging. This microscope has been successfully applied to different bacteria. EUV ptychography, complementing existing bio-imaging methods, requires straightforward, label-free preparation and provides novel insights into the structure and composition of microorganisms. In the future, extending the illuminating photon energy of a table-top EUV/X-ray source will enable the uncovering of structural and functional information of subcellular features in both dry and natural states (i.e., the water window).

3. References

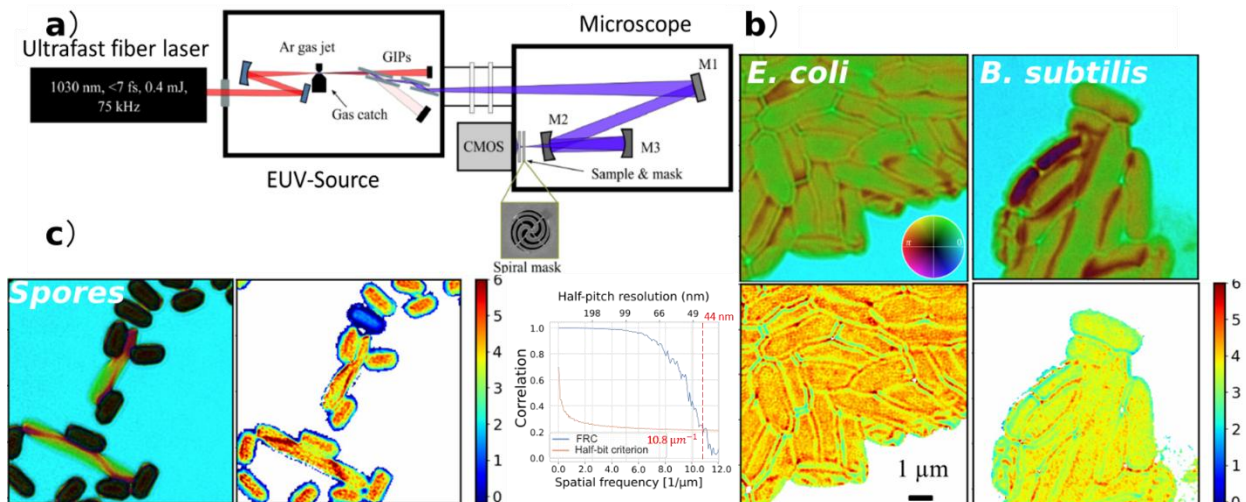


Figure 1: a) Table-top EUV ptychography setup. b) Reconstructed complex transmission and scattering quotient of *E. coli* and *B. subtilis* clusters. c) Reconstructed complex transmission and scattering quotient of *B. subtilis* treated with $MnSO_4$. The bacteria is spore-forming. Multiple spores with thicker protein layers are observed, some residue mother bacteria shows quite diverse properties under sporulation process. Fourier ring correlation indicates a diffraction limited half-pitch resolution of 44 nm.

- [1] J. Rothhardt, et al. "Table-top nanoscale coherent imaging with XUV light." *Journal of Optics* **20**.11 (2018): 113001.
- [2] B. L. Henke, et al., "Atomic data and nuclear data tables." **54.2**, 181-342, (1993).
- [3] J. Rodenburg, A. Maiden, "Ptychography." In *Springer Handbook of Microscopy*. Springer Handbooks. Springer, Cham. (2019).
- [4] P. D. Baksh, et al., "Quantitative and correlative extreme ultraviolet coherent imaging of mouse hippocampal neurons at high resolution." *Science advances*, **6**(18), eaaz3025 (2020).
- [5] C. Liu, et al. "Visualizing the ultra-structure of microorganisms using table-top extreme ultraviolet imaging." *Photonix* **4**, 6 (2023).
- [6] W. Eschen, et al., "High-speed and wide-field nanoscale table-top ptychographic EUV imaging and beam characterization with a sCMOS detector," *Opt. Express* **31**, 14212-14224 (2023)
- [7] T. J. Beveridge, et al., "Cellular responses of *Bacillus subtilis* and *Escherichia coli* to the Gram stain." *J Bacteriol.* **156**(2): 846-58 (1983)
- [8] R. Klas, et al., "Generation of coherent broadband high photon flux continua in the XUV with a sub-two-cycle fiber laser," *Opt. Express* **28**, 6188-6196 (2020)
- [9] W. Eschen, et al., "Structured illumination ptychography and at-wavelength characterization with an EUV diffuser at 13.5 nm wavelength," *Opt. Express* **32**, 3480-3491 (2024)
- [10] L. Loetgering, et al., "PtyLab.m/py/jl: a cross-platform, open-source inverse modeling toolbox for conventional and Fourier ptychography," *Opt. Express* **31**, 13763-13797 (2023)
- [11] W. Eschen, et al., "Material-specific high-resolution table-top extreme ultraviolet microscopy." *Light Sci Appl* **11**, 117 (2022).
- [12] S. Stöckel, et al., "Effect of supplementary manganese on the sporulation of *Bacillus* endospores analysed by Raman spectroscopy." *J. Raman Spectrosc.*, **40**: 1469-1477 (2009).

IR-DOSY (Infrared- Diffusion Ordered Spectroscopy): Adding the size dimension to spectroscopy

Carolyn J. Moll*, Giulia Giubertoni, Gijs Rombouts, Federico Caporaletti, Antoine Deblais, Rianne van Diest, Joost N. H. Reek, Daniel Bonn, and Sander Woutersen

*Van 't Hoff Institute for Molecular Sciences, University of Amsterdam, Science Park 904, 1098XH Amsterdam, The Netherland

Abstract:

Characterizing the size and the chemical structure of molecules and particles is essential in many research fields, including chemical synthesis, and quality control in pharmaceutical companies. Infrared (IR) spectroscopy is widely used as an analytical tool for chemical analysis due to its affordability and wide applicability. While IR spectroscopy provides information about the chemical structure of molecules, it lacks information about the size. Inspired by Nuclear Magnetic Resonance Diffusion-Ordered Spectroscopy (NMR-DOSY), which relies on the Stokes-Einstein relation that links the molecule's diffusion coefficient with its size, we have invented IR Diffusion-Ordered Spectroscopy (IR-DOSY). Using this technology, we can simultaneously characterize the molecular structure and the size of molecules and particles, thus adding another dimension to traditional one-dimensional infrared spectroscopy. The combined IR-frequency and diffusion-coefficient sensitivity is achieved by creating a concentration gradient within a newly developed sample cell, and tracking its equilibration in an IR-frequency resolved manner. From the acquired data a two-dimensional IR-DOSY spectrum can be constructed that has the IR-frequency on one axis and the diffusion coefficient (or equivalently, size) on the other axis. The IR-DOSY sample-cell can be easily integrated in any IR-spectrometer, transforming it into a size-sensitive tool.

[1] Infrared Diffusion-Ordered Spectroscopy Reveals Molecular Size and Structure; G. Giubertoni, G. Rombouts, F. Caporaletti, A. Deblais, R. v. Diest, J. N. H. Reek, D. Bonn, S. Woutersen ; *Angew. Chem.Int. Ed.* 2023, 62, e202213424

2-minute YouTube video summarizing the technology presented in our paper:
[YouTube IR-DOSY](#)

Fiber optic tapers for local biological detection

T. Martan, I. Kopacek, V. Prajzler*

* Corresponding author:

Tomas Martan, Czech technical university in Prague, Faculty of Electrical Engineering, Department of Microelectronics, Technická 2, 166 27 Prague, Czech Republic, E-mail: tomas.martan@fel.cvut.cz; Tel.: +420 224312264.

Ilja Kopacek, Czech technical university in Prague, Faculty of Electrical Engineering, Department of Microelectronics, Technická 2, 166 27 Prague, Czech Republic, E-mail: kopacilj@fel.cvut.cz; Tel.: +420 224312264.

Vaclav Prajzler, Czech technical university in Prague, Faculty of Electrical Engineering, Department of Microelectronics, Technická 2, 166 27 Prague, Czech Republic, E-mail: vaclav.prajzler@fel.cvut.cz; Tel.: +420 224312338.

Abstract

We would like to present results of our research that is focused on properties of optical fibers with polymer layers. Our current research deals with tapered optical fibers (fiber tapers), which we use in reflective or transmission configurations as sensors for biological applications.

Our poster presentation consists of two parts according to the arrangement of the sensor (reflective/transmission), resp. according to its application. The first one is focused on a fiber taper sensor equipped with an optical-chemical transducer incorporated in a polymer matrix intended for local detection of carbon dioxide (the fiber optic sensor in the reflective arrangement). The second part is focused on the fiber optic sensor in the transmission arrangement based on fiber taper with functionalized surface intended for virus detection.

1. Fiber optic tapers of single-cell dimensions for local carbon dioxide detection

This part of presentation includes the design, production and results of testing of the sensor for the local detection of gaseous carbon dioxide which dimensions is in units of micrometers. The sensor is based on a fiber taper tip covered by CO₂ sensitive dyed polymer layers. The dimensions of taper tip correspond to single-cell proportions that can be used in biological research, e.g. for testing of microorganisms and cells that actively consume gaseous carbon dioxide. The sensor principle is based on the absorption of guided visible light (numerically simulated modes propagation) in a sensitive polymer layer that reacts on carbon dioxide concentration. The sensor was tested from 0%-10.6% of carbon dioxide concentration with full linearity. The CO₂ measuring range was more than 10 times higher than the range of commercially available CO₂ detectors. A sensitivity of $0.25 \pm 0.05 \text{ dB/\%}$ and a limit of detection of $7.1 \cdot 10^{-3} \%$ have been determined for the sensing element. We have experimentally verified the operational reversibility of the CO₂ sensing element over time. The time response of the fiber optic sensor with the optimal sensitive polymer layer of thickness of 600 nm was one second.

2. Fiber optic tapers with functionalized surface for virus detection

The second part of our presentation is focused on the fiber optic sensor in the transmission arrangement based on fiber tapers with functionalized surface intended for virus detection.

The broadband (supercontinuum) light source and tapered optical fibers were primarily used for different virus detection. This research was inspired by the worldwide spread of COVID-19 disease. At that time, we had just started the development of a new fast and reliable fiber optic method for the detection of the corona virus SARS-CoV-2. First of all, we designed the detection principle (method) and then we produced a probe prototype. Then we developed measurement methodology that we tested first on E. coli bacteria and later on viruses less dangerous compared to corona virus SARS-CoV-2. Prepared fiber optic probes have been further tested on baculovirus in TNMH medium for SF9 insect cells, baculovirus in Insect express synthetic medium without the addition of SF9 bovine serum for insect cells, and finally on mouse polyomavirus in DMEM medium for mammalian 3T6 cells. Graphical outputs from the measurement of these viruses will be shown in a poster presentation.

All fiber optic sensors were produced on the optical fiber glass processor Vytran GPX-3000. Deposition of polymers on the fiber taper tips by dip-coating technique were performed in the NANOLAB

laboratory (Laboratory of Nanoelectronic Technologies) at the Department of Microelectronics, Faculty of Electrical Engineering, Czech technical university in Prague.

Keywords

Optical fiber, fiber taper, fiber tip, sensitive polymer layer, CO₂ detection, virus detection.

Acknowledgment

This work was supported by the research program of Czech Technical University in Prague within project no. SGS14/195/OHK3/3T/13.

References

- [1] Martan T., Mares D., Prajzler V., Local detection of gaseous carbon dioxide using optical fibers and fiber tapers of single-cell dimensions, *Sensors and Actuators B: Chemical*, Vol. 375 (2023).
- [2] Kopacek I., Martan T., Fraiberk M., Broadband light in optical fiber probes as the new “telescope” into sub-molecular bio-structures, *European Symposium on Ultrafast Laser driven Biophotonics, ESULAB 2022, Jena, Germany* (2022).
- [3] Chemnitz M., Zeisberger M., Schmidt M. A., Performance limits of single nano-object detection with optical fiber tapers, *Journal of the Optical Society of America B* 34 (9), 1833-1841 (2017).
- [4] Martan T., Komanec M., Zvanovec S., Preparation and Testing of Fiber Tapers for Repeatable Detection of Selected Hydrocarbons, *Advanced Photonics 2016 (OSA), Vancouver, Canada* (2016).
- [5] Martan T., J. Mrazek, S. Görlandt, Fiber-optic transmission system for CO₂ detection, *EUROPT(R)ODE XII, Athens, Greece* (2014).

Semi-stable supercontinuum generation for fast spectroscopy

MohammadSadegh Vafaeinezhad^{*a}, Tobias Meyer-Zedler^b, Michael Schmitt^a, Jens Limpert^a, Jürgen Popp

^a Friedrich Schiller University, Albert-Einstein-Straße 6, 07745 Jena, Germany ; ^bLeibniz-IPHT, Albert-Einstein-Straße 9, 07745 Jena, Germany

ABSTRACT

Supercontinuum sources are critical tools for spectroscopy applications. Hollow core fibers can deliver several microjoules (μJ s) of energy with a bandwidth covering from 200 to 4000 nm [1]. However, the solitonic nature of the supercontinuum in these fibers results in considerable instability. In contrast, recent advancements in all-normal dispersion (ANDi) fiber designs have achieved stable broadband supercontinuum spanning from 670 to 1390 nm [2]. Despite this progress, the small core diameter of ANDi fibers significantly restricts the pulse energy and, consequently, the power in these fibers. In this study, we explore a novel approach to supercontinuum generation aimed at mitigating instability at high pulse energies (>20 nJ). As illustrated in Figure 3, reducing instability can decrease the necessary pixel dwell time by a factor of seven. This development holds promise for the advancement of faster spectroscopy systems.

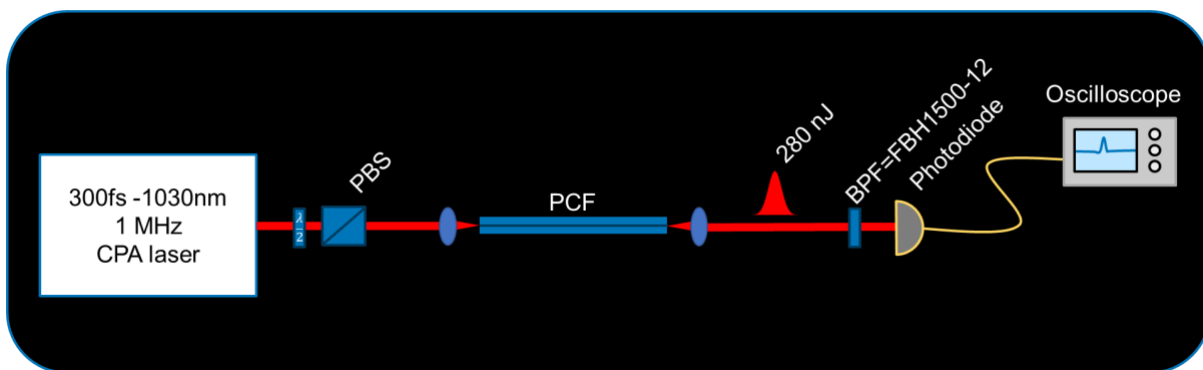


Figure 1. supercontinuum is pumped at 1030 nm and the stability is measured in a 12nm window around 1500 nm.

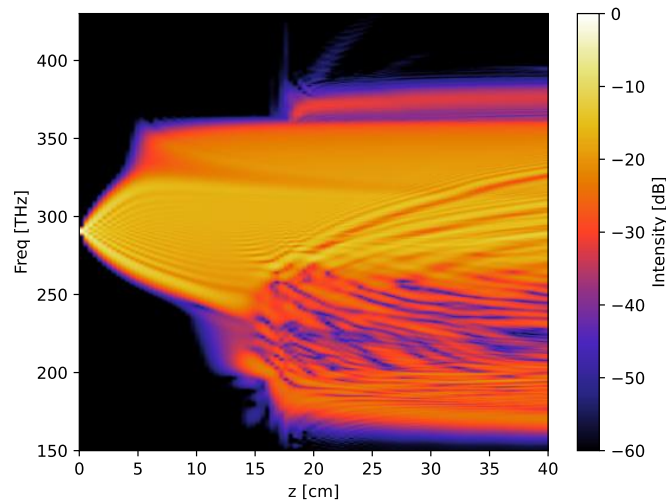


Figure 2. intensity of Supercontinuum generation

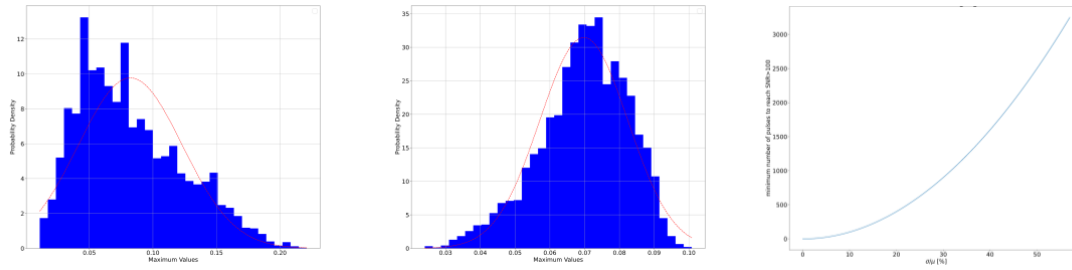


Figure 3. (left) histogram of measured pulse energies of an unstable supercontinuum system ($\sigma/\mu = 50\%$) (middle) histogram of measured pulse energies with reduced instability ($\sigma/\mu = 18\%$) (right) (calculated from theory) number of pulses that needs to be averaged to reach a SNR > 100 as a function of σ/μ of the supercontinuum source

ACKNOWLEDGEMENTS

MohammadSadegh Vafaeinezhad is part of the Max Planck School of Photonics supported by the German Federal Ministry of Education and Research (BMBF), the Max Planck Society, and the Fraunhofer Society. Also Funding from the Carl Zeiss Stiftung is greatly acknowledged.

REFERENCES

- [1] Genier, Etienne, et al. "Ultra-flat, low-noise, and linearly polarized fiber supercontinuum source covering 670–1390 nm." *Optics Letters* 46.8 (2021): 1820-1823.
- [2] Adamu, Abubakar I., et al. "Deep-UV to mid-IR supercontinuum generation driven by mid-IR ultrashort pulses in a gas-filled hollow-core fiber." *Scientific reports* 9.1 (2019): 4446.

Illuminating drug delivery: Localization and characterization of polymer-based nanoparticles in fibrotic liver cells

Julian Plitzko^{a,b}, Franziska Adermann^{c,d}, Thorben Köhler^{c,d}, Klea Mehmetaj^{d,e}, Stephanie Schubert^{c,d}, Adrian T. Press^{d,f,g}, Michael Schmitt^a, Michael Bauer^{d,e,g}, Juergen Popp^{a,b}

^a Institute of Physical Chemistry and Abbe Center of Photonics, FSU Jena; ^b Leibniz Institute of Photonic Technology (IPHT), Member of Leibniz Health Technologies, Member of the Leibniz Centre for Photonics in Infection Research (LPI); ^c Laboratory of Organic and Macromolecular Chemistry (IOMC), FSU Jena; ^d Jena Center of Soft Matter (JCSM), FSU Jena; ^e Department of Anesthesiology and Intensive Care Medicine, Jena University Hospital; ^f Faculty of Medicine, Friedrich Schiller University Jena; ^g Center for Sepsis Control and Care, Jena University Hospital;

A promising way to address liver fibrosis is to utilize functionalized polymer-based nanoparticles (NPs) to target the natural vitamin A receptor of liver cells, STRA6 (stimulated by retinoic acid 6). Those NPs are designed to encapsulate drugs in the necessary concentration to inhibit the signalling pathway inside the hepatic stellate cells that are responsible for inflammation.

To investigate the NPs within cells and tissue, molecular selective microspectroscopic techniques are well suited. Here, we report about the application of Raman microscopy (Fig.1a), confocal fluorescence microscopy (Fig.1b), and coherent anti-Stokes Raman scattering (CARS) microscopy (Fig.1c) to study the localization of NPs in liver cells and tissue. Furthermore, Raman spectroscopy in combination with two-dimensional correlation analysis (2DCOS) is utilized for the characterization of polymers, NPs, and drugs prior to their analysis in biological environments. Such a detailed Raman spectroscopic analysis of the polymers and the corresponding NPs allows for the identification of characteristic vibrations that enables a label-free localization of the NPs by CARS microscopy within cells. Fluorescence-lifetime imaging microscopy (FLIM) providing insights into the release of the encapsulated drugs out of the NPs has also been applied (Fig.1d).

These microspectroscopic approaches are aimed for a spatiotemporal localization of the NPs and is supported by tailor-made image analysis routines to further characterize the NP uptake processes and induced metabolic influence.

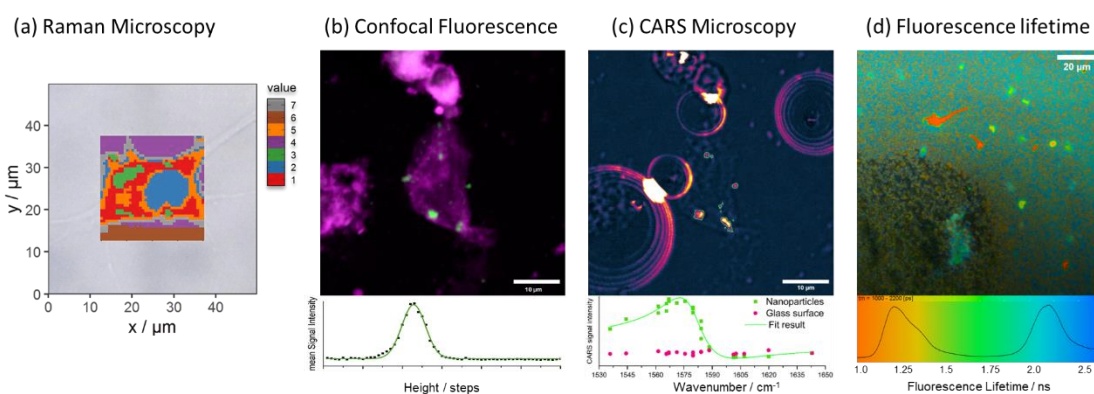


Figure 1: A variety of linear and non-linear modalities can be utilized to localize and characterize polymer-based nanoparticles inside of cells and tissue.

ACKNOWLEDGMENTS

This study was funded by the German Research Foundation (DFG) through the Collaborative Research Centre PolyTarget 1278 "Polymer-based nanoparticle libraries for targeted anti-inflammatory strategies" (project C01) under DFG project number 316213987.

Fabrication of High-NA Microlenses by Two-photon polymerization(2PP) for Linear and Non-linear Microscopy

Behjat S. Kariman^{1,*}, *Alessandra Nardini*², *Mario Marini*³, *Claudio Conci*², *Manuela T. Raimondi*², *Roberto Osellame*⁴, *Giuseppe Chirico*³, *Giulio Cerullo*¹ and *Rebeca Martínez Vázquez*⁴

¹Department of Physics, Politecnico di Milano, Milan, Italy

²Department of Chemistry, Materials and Chemical Engineering “Giulio Natta”, Politecnico di Milano, Milan, Italy

³Department of Physics, Università degli Studi di Milano-Bicocca, Milan, Italy

⁴Institute for Photonics and Nanotechnologies (IFN), CNR, Milan, Italy

Behjatsadat.kariman@polimi.it

3D in vivo deep-tissue imaging requires a sophisticated optical system with innovative approaches to mitigate light scattering and specimen-induced aberrations observed in biological tissues [1]. Tissue-scattering limits the penetration depth of available imaging techniques and impacts image quality. Non-linear approaches (such as SHG, THG, TPEF, SRS, etc.) enable high penetration depth and reduce scattering due to the use of near-infrared radiation [1, 2]. Nevertheless, spatial resolution is low in deep-tissue imaging also because of spherical aberrations induced on highly focused beams (large NA) into the tissue. In this context, we propose a high dioptric power microlenses to be coupled with a low numerical aperture objective lens onto an imaging system, to reduce spherical aberrations. These microlenses are fabricated using the combination of two-photon photon polymerization and UV exposure [3]. We explored high NA aspherical parabolic microlenses with varying focal lengths, to optimize the imaging characteristic. We optimized the entire process to minimize fabrication time while preserving the robustness and the optical quality of the structures. The use of a parabolic shape allows us to increase the size of the microlenses with respect to conventional plano-convex lenses. Our results indicate that these microlenses are wide enough to be utilized on both linear and non-linear excitation imaging modes. Since they are made of biocompatible photoresist SZ2080, we envisage that they can even be implanted in tissue to reduce spherical aberrations for in-vivo imaging.

[1] V. N. Astratov. "Roadmap on Label-Free Super-Resolution Imaging, " *Laser Photonic Review*, 17, (2023).

[2] C.J.R. Sheppard. "Multiphoton Microscopy: a personal historical review with some future prediction," *Biomed. Opt.*, (2020).

[3] M. Marini., et al. Microlenses Fabricated by Two-Photon Laser Polymerization for Cell Imaging with Non-Linear Excitation Microscopy, *Adv. Funct. Mater.*, 2213926 (2023).

Acknowledgments

This project has received funding from the European Union’s Horizon 2020 research and innovation programme under grant agreements No 964481.

Fluorescence Lifetime Spectroscopy using Entangled Photons from a Continuous-Wave Source

Tobias B. Gäbler and Valerio F. Gili

Fraunhofer Institute of Applied Optics and Precision Engineering IOF, Albert-Einstein-Straße 7, D-07745 Jena, Germany
E-Mail: tobias.bernd.gaebler@iof.fraunhofer.de

Abstract: Our study addresses the applicability of entangled photons for fluorescence lifetime spectroscopy. We show the proof that the determination of fluorescence lifetimes depending on the excitation wavelength is feasible by using a CW-pump entangled photon pair source.

1. Introduction

Fluorescence lifetime imaging microscopy (FLIM) is one of the work horses in chemistry, biology, and medicine. Several methods for FLIM are established, mainly based on pulsed illumination or phase modulation. These methods require a high technical effort connected the risk of photobleaching. Quantum light provides the opportunity to avoid this disadvantage: Because of the intrinsic time-frequency correlation of entangled photons, a minimal light intensity is sufficient for the determination of the fluorescence lifetime without the use of pulsed laser sources [1]. Moreover, it was already shown that quantum light enables a higher temporal resolution than conventional FLIM methods [2].

Entangled light generated by spontaneous parametric down-conversion (SPDC) in nonlinear waveguides offers an additional benefit for FLIM: Entangled photons with narrow bandwidths and easily manageable center wavelengths. With this, spectral resolved investigations of fluorescence lifetimes without cost-intensive tunable light sources are possible.

2. Experimental Method

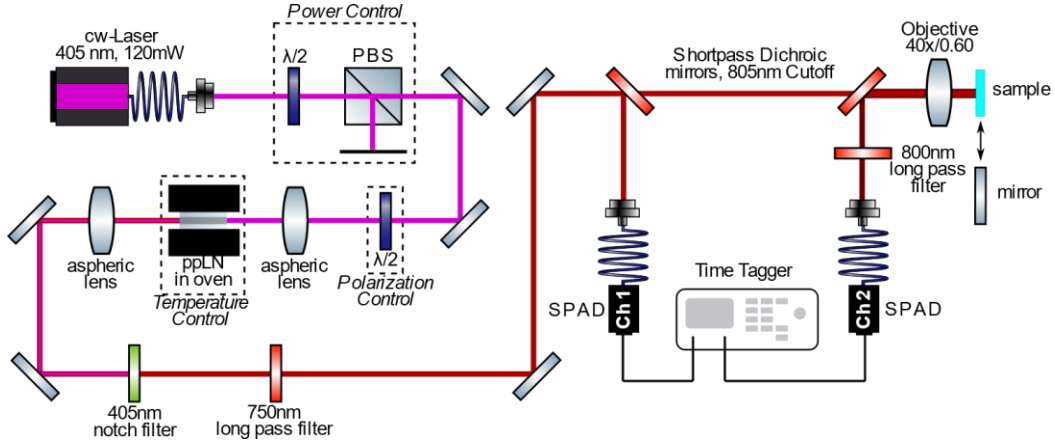


Fig. 1: Scheme of the experiment FLIM setup based on quantum light.

In our study, we use a highly efficient photon pair source based on CW-pumping of a periodically poled lithium niobate waveguide (fig. 1) [3]. After its generation, the beam of an entangled photon pairs is guided to a self-made microscope equipped with two single photon avalanche diodes (SPAD) and a time counting unit. By the help of the first dichroic mirror, the entangled photons will be separated spectrally. In doing so, the photon with wavelength above 805nm triggers the photon counting (detector Ch1), whereas the corresponding photon with a wavelength below 805nm excites the fluorescence sample (IR-140) by single-photon absorption. This excitation introduces a temporal delay between trigger photon and the emitted fluorescence photon, which will be guided to the second detector (Ch2). For this reason, time-correlation function $\tilde{F}(t)$ of trigger and fluorescence photons is related to the fluorescence decay. However, according to eq. (1), the real fluorescence decay $F(t)$ is convolved with the instrumental response function (IRF), which contains the delay due to the light propagation in the setup.

$$\tilde{F}(t) = IRF(t) * F(t) \quad (1)$$

The IRF can be determined by replacing the sample with a mirror so that the entangled photons with a wavelength above 805nm are back reflected to the second dichroic mirror. Due to the imperfectness of the dichroic mirror, a small amount of these photons is guided to detector Ch2. Removing the long pass filter before detector Ch2 enables the measurement of the IRF by correlating the residual photons with the trigger photons.

The necessary deconvolution of eq. (1), and with that the determination of fluorescence lifetime τ , is performed by a numerical parameter optimization with assuming a fluorescence decay in the form of

$$F(t) = F_0 \cdot \exp(-t/\tau). \quad (2)$$

3. Results

We investigate IR-140 solved in ethanol to proof the applicability of fluorescence lifetime spectroscopy using entangled photons. For this purpose, the correlation histograms $IRF(t, \vartheta)$ and $F(t, \vartheta)$ are recorded for several waveguide temperatures ϑ between 63°C and 75°C. These temperatures are directly related to excitation wavelengths of from 800nm down to 760nm because of the energy conservation during the SPDC process (fig. 2 left).

Our preliminary results show fluorescence lifetimes $\tau(\vartheta)$ in the order of 1ns (fig. 2 right), which is comparable with reported values for IR-140 in ethanol [4]. A dependency on the waveguide temperature ϑ is observable, which may result from the molecular properties. In a next step, we intend to increase the temporal resolution as shown in ref. [2] to reduce the visible uncertainty.

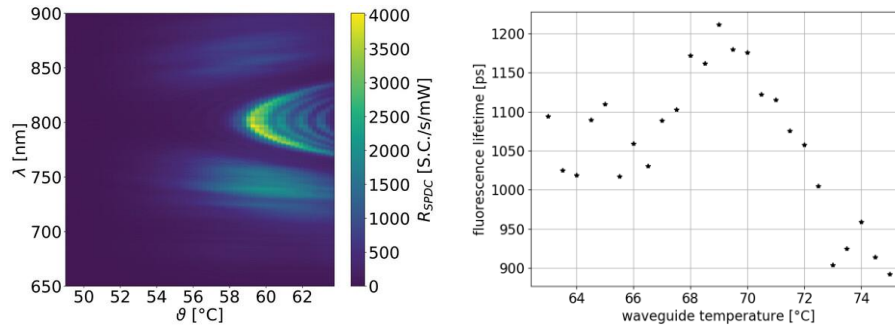


Fig. 2: Left: single photon spectra of similar waveguide photon pair source for different temperatures T [3]; Right: fluorescence lifetimes $\tau(T)$ of IR-140 determined using CW entangled photon pairs.

4. References

- [1] A. Eshun et al., Opt. Express **31**, 26935-26947 (2023).
- [2] N. Harper et al., J. Phys. Chem. Lett. **14**, 5805-5811 (2023).
- [3] T. B. Gäbler et al., Adv. Phys. Res. **3**, 2300037 (2024).
- [4] C. L. Hutchinson et al., Appl. Opt. **35**, 2325-2332 (1996)

LINCam: principle, applications and perspectives of wide-field time correlated single photon counting

André Weber¹, Yury Prokazov², Evgeny Turbin², Nikhil Tiwari¹, Rodrigo Herrera-Molina¹, Nazar Oleksiievets³, Roman Tsukanov³, Artur Bikbaev⁴, Stefan Richter¹, Oliver Kobler¹, Werner Zuschratter¹

¹ Combinatorial NeuroImaging Core Facility, Leibniz-Institut für Neurobiologie, Brennekestr. 6, 39118 Magdeburg.

² Photonscore GmbH, Brennekestr. 20, 39118 Magdeburg.

³ III. Institute of Physics – Biophysics, Georg August University, 37077 Göttingen.

⁴ Institut für Entwicklungsbiologie und Neurobiologie (iDN) Funktionelle Neurobiologie - AG Heine, Johannes Gutenberg-Universität Mainz, Hanns-Dieter-Hüsck-Weg 15, 55128 Mainz, Germany.

Current fluorescence microscopy often requires relatively high doses of light, which can harm living specimens due to photon damage. We introduce an alternative approach using a wide-field imaging technique with a highly sensitive detector. Our system utilizes a position-sensitive detector with multichannel plates for electron amplification (LINCam, Photonscore GmbH), and operates based on single-photon counting. Using new photocathodes characterised by high quantum efficiency and exceptional signal-to-noise ratio, our system allows imaging under very low light conditions ($< 30\text{mW/cm}^2$) and generates diffraction-limited FLIM images by capturing the position and timing information of individual light quanta in a continuous data stream. This method offers a positional accuracy akin to a 1000×1000 pixel camera with a time accuracy of 40 ps, facilitating long observation times for sensitive samples. Its applications span calcium imaging, single molecule detection, FLIM-FRET, and quantum optics. Additionally, it enables label-free imaging of metabolic processes by detecting autofluorescence from metabolites like NADH and FAD, promising new avenues for studying cellular and tissue vitality under pharmacological stress and distinguishing between healthy and diseased tissue in medical diagnostics. Moreover, the system can simultaneously gather multimodal data from multiple detectors and can be expanded with a spectrometer into a hyperspectral time-resolved Raman FLIM imaging system.

Imaging of a trapped ion crystal via Intensity interferometry

Stefan Richter^{1,2}, **Sebastian Wolf**³, **André Weber**², **Joachim von Zanthier**¹, **Ferdinand Schmidt-Kaler**³

¹Institut für Optik, Information und Photonik, Friedrich-Alexander-Universität Erlangen-Nürnberg, Staudtstr. 1, 91058 Erlangen, Germany

²Combinatorial NeuroImaging Core Facility (CNI), Leibniz

Institute for Neurobiology Magdeburg, Brenneckestraße 6, 39118 Magdeburg, Germany

³QUANTUM, Institut für Physik, Johannes Gutenberg-Universität Mainz, Staudingerweg 7, 55128 Mainz, Germany

We measured the second order spatio-temporal correlation function for the light spontaneously emitted from a trapped and laser-cooled two-ion crystal. In the temporal regime, the $g^{(2)}(\tau)$ auto-correlation signal shows bunching or antibunching for different observer positions [1]. Using two position sensitive Micro Channel Plate detectors (MCP) developed for applications in fluorescence lifetime microscopy combining excellent spatial resolution with high temporal resolution, we also measured the spatial cross-correlations of the fluorescence light. In this way, we implemented intensity interferometry for the light scattered by a two-ion crystal. In fact, the complete spatial-temporal modulation of $g^{(2)}(\vec{x}_1, \vec{x}_2, \tau)$, predicted in [2] for two trapped atoms, can now be measured with two MCPs by recording the corresponding two photon events for any time difference $\Delta\tau$ and position pairs x_1 and x_2 . After the event stream is recorded, the cross-correlations can be reconstructed to image the trapped ion crystals [3,4] and investigate the cooperative emission behaviour of the trapped ion crystal.

[1] S. Wolf et al. Phys. Rev. Lett. 124, 063603 (2020)

[2] C. Skornia et al., Phys. Rev. A 64, 063801 (2001)

[3] S. Richter et al., Phys. Rev. Lett. 126, 173602 (2021)

[4] S. Richter et al., Phys. Rev. Research. 5, 013163 (2023)

Ultrafast Oscillators and Amplifiers for Physics and Chemistry

Dr. Brian Molesky, Dr. Erin McCole Dlugosz, Dr. Joseph Henrich

Coherent Corp, West of Scotland Science Park, Maryhill Rd, Glasgow G20 0XA, UK
Brian.molesky@coherent.com, erin.dlugosz@coherent.com

Abstract: Created by the *Industrial Revolution in Ultrafast Science*, Coherent offers ultrafast lasers for research applications, with pulse energies from μJ to mJ , repetition rates into the MHz regime, at wavelengths from UV to mid-IR.

Main Text

Research applications using ultrafast lasers have one thing in common – the lasers should be available whenever you need them. It's that simple. Recognizing that reliability and lifetime are just as important as cutting-edge performance, Coherent pioneered the Industrial Revolution in Ultrafast Science by investing in equipment and processes to bring uptime to new heights.

The Industrial Revolution in Ultrafast Science. The Coherent Solution

In order to make ultrafast pulses accessible to the broadest possible field of applications in physics and chemistry, Coherent has been implementing a comprehensive program of design methodologies, materials qualification and sourcing and HALT/HASS testing protocols that go under the name of the *Industrial Revolution in Ultrafast Science*. This approach emphasizes performance, operational simplicity, repeatability and reliability.

Rigorous HALT/HASS Stress Testing

Coherent was the first laser manufacturer to invest in HALT/HASS testing equipment and utilize rigorous screening protocols. We stress and test our lasers over and over to ensure you get the superior performance and reliability your research needs. HALT (Highly Accelerated Lifetime Testing) is critical during the development phase of our products, while HASS (Highly Accelerated Stress Screening) is used throughout the manufacturing process. The “HASS Verified” emblem on our lasers is the visible assurance that each product meets our HASS reliability testing requirements.

Vertical Integration

We design and make all the critical components and sub-systems in-house for our ultrafast lasers, and we only use materials that we have been qualified in our facilities. This gives us full control over the quality of all critical components and subsystems. The result is superior performance and reliability.

Industrial Laser Experience

Coherent is the world's leading manufacturers of industrial lasers for both heavy-duty industrial applications and precision microelectronic manufacturing, where 24/7 reliability is mandatory. We draw on that experience to bring you the performance and reliability you deserve.

Ultrafast laser performance with industrial reliability.

With an unmatched laser amplifier portfolio offering pulse energies from $40 \mu\text{J}$ to 9mJ , and repetition rates from 1 kHz to 50 MHz, Coherent can supply every part of your ultrafast laser system: pump lasers (Revolution), oscillators (Vitara), amplifiers (Astrella, Monaco), tunable OPAs (TOPAS Prime, OperaSolo, Opera-F), and accessories (harmonic generators).

References

[1] <https://www.coherent.com>

[2] https://www.coherent.com/resources/brochures/lasers/COHR_IndustrialRevolutionBrochure_1020_5.pdf